

TERAHERTZ TRANSMISSION ENHANCEMENT IN
FINITE-SIZE ARRAYS OF SUBWAVLENGTH HOLES
MODIFIED WITH DIELECTRIC PEG LAYER

By

BRADY ANDREW WHISENHUNT

Bachelor of Science in Electrical Engineering

Oklahoma State University

Stillwater, Oklahoma

2005

Submitted to the Faculty of the
Graduate College of the
Oklahoma State University
in partial fulfillment of
the requirements for
the Degree of
MASTER OF SCIENCE
May, 2013

TERAHERTZ TRANSMISSION ENHANCEMENT IN
FINITE-SIZE ARRAYS OF SUBWAVLENGTH HOLES
MODIFIED WITH DIELECTRIC PEG LAYER

Thesis Approved:

Dr. Weili Zhang

Thesis Adviser

Dr. Daniel Grischkowsky

Dr. Charles Bunting

Name: BRADY ANDREW WHISENHUNT

Date of Degree: MAY, 2013

Title of Study: TERAHERTZ TRANSMISSION ENHANCEMENT IN FINITE-SIZE
ARRAYS OF SUBWAVELENGTH HOLES MODIFIED WITH
DIELECTRIC PEG LAYER

Major Field: ELECTRICAL ENGINEERING

ABSTRACT:

Scope and Method of Study: This thesis investigates terahertz transmission through finite-size arrays of subwavelength holes perforated in a thin aluminum film modified with a periodic layer of dielectric pegs resting on the hole openings. Samples of differing patterns and numbers of holes were fabricated in a 350 nm thick layer of aluminum on top of a 640 μm thick silicon substrate layer. The dielectric peg layer (DPL) consisted of periodically-spaced pegs composed of negative photoresist material. Terahertz time-domain spectroscopy measurements of the transmission were taken both before and after fabrication of the DPL on top of the hole array samples. The results were analyzed and compared to simulation of an infinitely periodic hole array modified with a DPL.

Findings and Conclusions: A peak in the transmission spectrum was observed at the predicted surface plasmon resonance frequency for the array. The transmission peak was enhanced 5%-20% with addition of the DPL, depending on the arrangement and number of holes in the sample. A weaker peak was observed in some samples at higher frequencies with addition of the DPL, which is attributed to a resonance of the DPL layer itself. Both the resonant and nonresonant components of transmission were enhanced with addition of the DPL. Simulation showed a similar enhancement of the resonant and nonresonant transmission due to DPL. Varying the value of the dielectric constant of the simulated pegs changed the strength of the fundamental surface plasmon resonance as well as the location of the higher frequency peaks. A Fano-like asymmetry was observed in the experimentally measured transmission spectra but not observed in simulation. The results suggest that a heterostructure consisting of a finite-size array of subwavelength holes combined with a DPL can be used to enhance the transmission of light through the holes as well as tune the asymmetry of the main surface plasmon resonance peak.

TABLE OF CONTENTS

Chapter	Page
I. INTRODUCTION.....	1
1.1 Electromagnetic Waves Near Small Apertures	1
1.2 Extraordinary Optical Transmission.....	2
1.2.1 Surface Plasmon Polaritons	2
1.2.2 Subwavelength Hole Arrays.....	6
1.3 Terahertz Plasmonics.....	9
1.4 Outline of This Thesis	12
II. BACKGROUND	13
2.1 Surface Plasmons on Infinitely Periodic Textured Surfaces	14
2.2 Transmission Through Finite-Size Subwavelength Hole Arrays.....	16
2.2.1 Numerical Modeling of Finite-Size Hole Arrays	17
2.2.2 Analytical Modeling of Finite-Size Hole Arrays	18
2.3 Resonances in Subwavelength Hole Arrays.....	22
2.3.1 Lattice and Superlattice Resonances	22
2.3.2 Plasmonic Oligomers, Hybridized Plasmons, and Fano Effects	24
III. DESIGN AND SIMULATION OF PLASMONIC HETEROSTRUCTURES	30
3.1 Design Considerations.....	30
3.1.1 Design of “h” Clusters.....	36
3.1.2 Design of “r” Clusters	38
3.1.3 Design of “rand” Clusters.....	38
3.2 Modeling the DPL Effect	40
3.2.1 Enhancement of the Main Resonance	42
3.2.2 Higher Frequency Features.....	48

Chapter	Page
IV. THZ-TDS EXPERIMENT	51
4.1 8F THz-TDS Beam System	51
4.2 Fabrication of Plasmonic Heterostructures	53
4.3 Data Acquisition	56
V. RESULTS OF EXPERIMENT	59
5.1 Transmission Spectra of Experimental Structures	59
5.1.1 Main Resonance Enhancement in “h” Clusters	62
5.1.2 Main Resonance Enhancement in “r” Clusters	67
5.1.3 Higher Frequency Features	70
5.1.4 Transmission Enhancement in “rand” Clusters	71
5.2 Comparison to Simulation	73
5.2.1 Enhancement of Main Resonance	73
5.2.2 Fano-like Characteristics of Main Resonance	73
VI. CONCLUSION	78
6.1 Summary of Results	78
6.2 Future Work	79
REFERENCES	81

LIST OF TABLES

Table	Page
5-1 Peak data for metal hole clusters without DPL	61
5-2 Peak data for metal hole clusters with DPL	64
5-3 Fano parameters extracted from peaks in Figure 5-9	77

LIST OF FIGURES

Figure	Page
1-1 Photograph of a subwavelength hole array	3
1-2 Schematic for a surface plasmon wave on a smooth metal surface	4
1-3 Plot of surface plasmon dispersion relation	7
1-4 Diagram of surface plasmon coupling through periodic hole array	8
1-5 Diagram comparing SP field confinement at light and terahertz frequencies....	10
2-1 Diagram of SP excitation through grating coupling effect	15
2-2 Schematic showing scattering events in a finite-size hole array	20
2-3 Examples of molecular-type resonances in a plasmonic trimer	25
2-4 Layout of a finite-size hole array with 37 holes.....	27
2-5 Illustration of Fano resonance tuning via plasmonic transmutation	29
3-1 Close-up illustrations of hole-peg combinations in the experimental samples..	31
3-2 Depiction of subwavelength hole array structure without DPL (to-scale).....	33
3-3 Depiction of subwavelength hole array structure with DPL (to-scale).....	34
3-4 To-scale views of DPL structure.....	35
3-5 Microscope image of mask patterns used to fabricate each hole array	37
3-6 Illustration of calculation methodology for “porosity” normalization constant	39
3-7 Schematic of boundary conditions used in specifying the simulation unit cell .	41
3-8 Simulated transmission spectra of array varying dielectric constant of pegs	43
3-9 Simulated E_z distribution at 0.58 THz	45
3-10 Simulated H_y distribution at 0.58 THz.....	46
3-11 Surface current distributions on both sides of metal surface at 0.58 THz	47
3-12 Simulated reflection spectra of array varying dielectric constant of pegs	49
3-13 Surface current distributions on both sides of metal surface at 2.04 THz	50
4-1 Schematic of 8F THz-TDS system used in experiment.....	52
4-2 Illustration of steps in fabricating holes arrays in metal film.....	54
4-3 Illustration of steps in fabricating NPR peg layer on top of hole arrays.....	55
4-4 Diagram showing laser beam axial intensity distribution and hole array	58
5-1 Comparison of normalized transmission in hole arrays without DPL	60
5-2 Comparison of normalized transmission in hole arrays with DPL	63
5-3 Plot of normalized transmission spectra of “h” samples before and after DPL .	65
5-4 Plot of peak transmission for “h” samples versus number of holes.....	66
5-5 Plot of normalized transmission spectra of “r” samples before and after DPL..	68
5-6 Plot of peak transmission for “r” samples versus number of holes.....	69
5-7 Plot of transmission spectra of aperiodic samples with and without DPL.....	72
5-8 Plot comparing simulated spectra and experimental data	74
5-9 Close-up plot of normalized transmission peaks for simulation and h127	76

CHAPTER I

INTRODUCTION

1.1 Electromagnetic Waves Near Small Apertures

One of the fundamental conclusions in classical electrodynamic theory is that the physical length associated with one period of a propagating electromagnetic plane wave largely determines how it interacts with an obstacle [1]. In the case of an aperture in a conducting thin metallic sheet, a limit is placed on how small the opening can be before the percent energy transmission is, for most practical purposes, negligible. When the aperture size drops below the “subwavelength” scale, the electrostatics at the interface is described largely by curvature of magnetic field through the gap as first reported by H.A. Bethe [2].

In practical settings, the matter of subwavelength transmission is more complicated. Indeed, Bethe’s calculations were rigorous for the simplified case of an infinitely thin, infinitely wide perfect electric conductor. However, as the conductor thickness increases, waveguide modes native to the hole shapes need to be accounted for [3-5]. As the infinite conductivity of the conductor is replaced with “real metal” behavior, dispersive phenomena are encountered [6, 7]. Altering hole shape at the nanoscale introduces excitation of different evanescent electromagnetic modes [8-11].

1.2 Extraordinary Optical Transmission

In 1998 [12] reported subwavelength transmission through subwavelength holes in a metal film far-exceeded the expectations predicted by the Bethe model. In fact, the magnitudes of the transmission amplitudes were so “anomalous” that the phenomena were quickly assigned the designation of Extraordinary Optical Transmission (EOT). Soon after, the EOT phenomena had been replicated in dozens of research groups across the world, and a wide range of research dealing with this specialized field of subwavelength optical effects has since sprung up [13-22]. Studies on numerous permutations of subwavelength aperture structures have been performed, resulting in new vistas of possibilities for use in the design of nanophotonic devices such as sensors [14, 16, 23-26], waveguides [27-29], beam shaping [24, 27, 28, 30-34], optical filters and switches [24, 35-37], microscopy [32], laser design [33, 34, 38], and even quantum systems [35, 39].

1.2.1 Surface Plasmon Polaritons

The general phenomenon of EOT in subwavelength hole arrays can be explained in terms of a concept known as surface plasmon (SP) or surface plasmon polariton (SPP). For the purposes of this study, the terms SP and SPP will be used interchangeably. A SPP can be understood as an electromagnetic surface wave that exhibits plasma-like propagation dynamics arising from the collective electron gas oscillations within certain real metals [6, 7]. These plasma-like waves can be excited by a variety of means, by exploitation of Drude dispersion in metals [19, 21, 40, 41].

Since the frequency-dependent dielectric constant of a real metal has both a real and imaginary component, the latter having a negative sign at high frequencies, there exist certain frequency ranges that bring about distinct types refractive characteristics. Consider the basic expression for the complex electric permittivity ϵ_r :

$$\epsilon_r(\omega) = \epsilon'(\omega) + i\epsilon''(\omega). \quad (1-1)$$

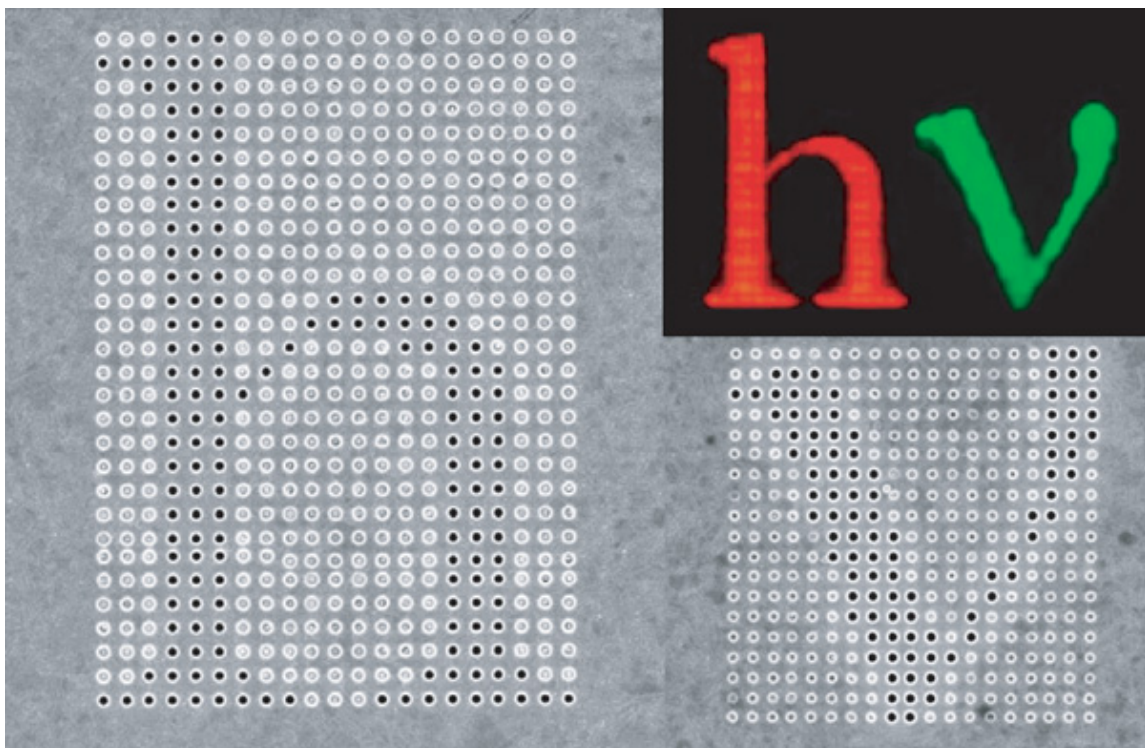


Figure 1-1 Demonstration of a subwavelength hole array used as an optical filter. The color of the transmitted light through the subwavelength holes (inset) is governed by the period of the square lattice of holes and dimples. The red “h” and green “v” have periodicities of 550nm and 450nm, respectively. From [22].

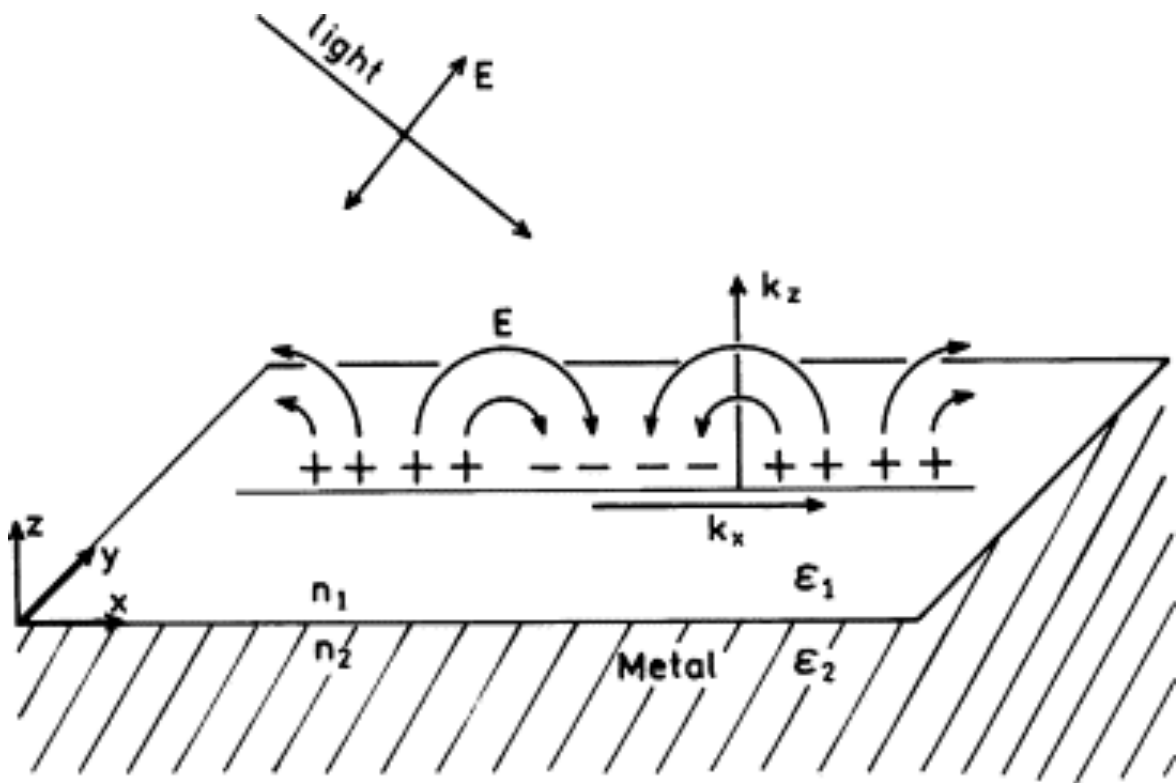


Figure 1-2 Schematic representation of surface plasmon wave on a smooth metal surface. Adapted from [42]

This quantity is used when solving time-harmonic electromagnetic field problems involving frequency-dependent dispersion [1], and in this it refers specifically to the propagation constant of an electromagnetic plane wave described by the general frequency-domain form:

$$\mathbf{E}_z = A e^{i(\omega t - kz)}. \quad (1-2)$$

In this case \mathbf{E}_z quantifies the electric field strength of a particular electromagnetic wave at a given angular frequency ω , at time t , with amplitude A , at position z along the z -axis in a 3-dimensional region. The wavevector k in Eq. (1-2) contains both frequency information about the wave as well as information about the media in which it is propagating, and is related to the speed of light by

$$k = \frac{\omega}{v} = \frac{\omega}{\sqrt{\epsilon\mu}}, \quad (1-3)$$

where v is the speed at which light propagates inside the material, and ϵ and μ denote the electric permittivity and magnetic permeability of the medium. So, the speed of light within a medium depends upon the frequency response of the dielectric constant of the material. The dispersive properties of metals at conventional frequencies are well-known by experimentation, and in the case of Drude metals, mathematical patterns in their dispersion curves have been identified [6] from experimentation. Though in many cases it is suitable to approximate the dielectric constant of a metal as a perfect electric conductor (PEC) with infinite conductivity, in cases dealing with possible surface plasmon effects, it is beneficial to take advantage of the Drude model's allowance of some penetration of field into the metal. As opposed to explicitly specifying the metal's permittivity frequency-by-frequency, one can obtain a satisfactory approximation by specifying two parametric constants: damping frequency ω_τ , and plasma frequency ω_p . These allow the complex permittivity ϵ_c to be expressed as a continuously differentiable function:

$$\epsilon_c = \epsilon_\infty - \frac{\omega_p^2}{\omega^2 + i\omega\omega_\tau}, \quad (1-4)$$

which may be split into its real and imaginary parts, ϵ_R and ϵ_I , respectively, so that the wavevector k from Eq. (1-3) may also be split into real and imaginary components. A complex

\mathbf{k}_{\parallel} for a wave traveling along a metal surface indicates a finite propagation length and an exponential decay of the field, due to the real component of the exponential term in Eq. (1-2).

A generalized dispersion relation for a surface plasmon at the interface between a Drude metal and a dielectric medium is illustrated by the plasma dispersion plot in [Figure 1-3](#). This figure describes the coupling conditions needed to excite a surface plasmon. The dispersion curve lies to the right of the constant-slope light line but below the plasma frequency defined by $\omega = \omega_p$. If \mathbf{k}_{\parallel} is sufficiently boosted for light at the plasma frequency, then the condition can be satisfied to couple the light into a surface plasmon wave at ω_p .

1.2.2 Subwavelength Hole Arrays

In subwavelength hole arrays, numerous tiny holes are drilled into a metal layer. In this configuration the momentum deficit for surface plasmon excitation is remedied by the grating effect formed by the periodically spaced holes. Constructive and destructive interference of the light scattered at the hole openings essentially selects certain frequencies to be boosted in intensity, and if these frequencies match ω_p for the metal hole array, then surface plasmons can be coupled to the surface of the metal. In general, the surface plasmon resonance frequency can be described as a function of the incident light and lattice constant of the hole array:

$$\mathbf{k}_{SP} = \mathbf{k}_{SP}^0 + \mathbf{k}_R = \frac{\omega}{c} \sqrt{\frac{\epsilon_d \epsilon_m}{\epsilon_d + \epsilon_m}} + \mathbf{k}_R, \quad (1-5)$$

where \mathbf{k}_{SP} is the surface plasmon wavevector, \mathbf{k}_{SP}^0 is the lowest order SP mode, and \mathbf{k}_R contains the wavevectors of the reciprocal lattice of the holes. The quantity \mathbf{k}_R is of critical importance to

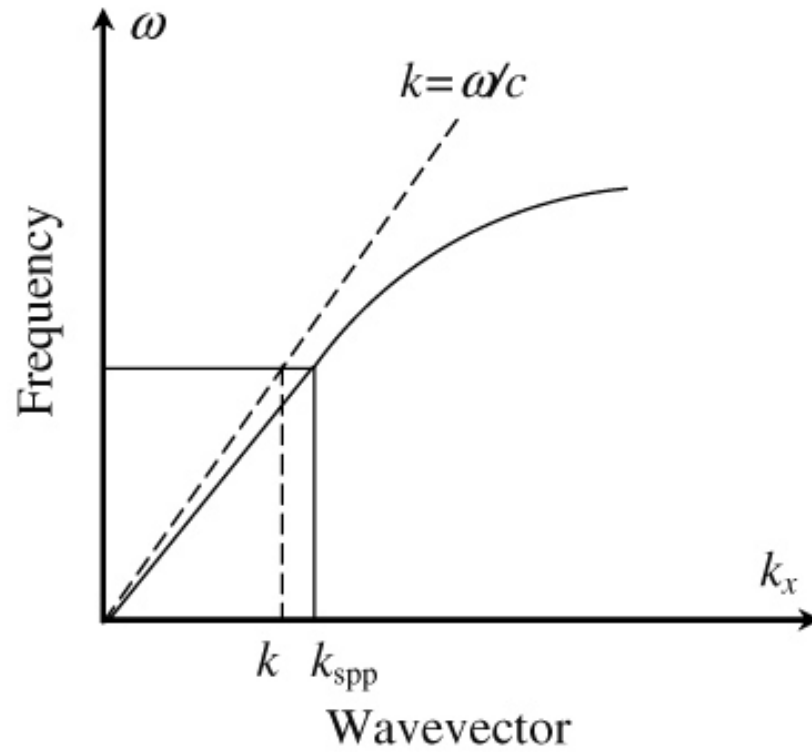


Figure 1-3 Dispersion relation for surface plasmon (SP). When the grating vector k_R provides sufficient momentum to a photon of frequency ω and wavevector k to meet the surface plasmon wavevector k_{SPP} (solid curve), a surface plasmon wave is excited, which propagates parallel to the metal surface. From [43]

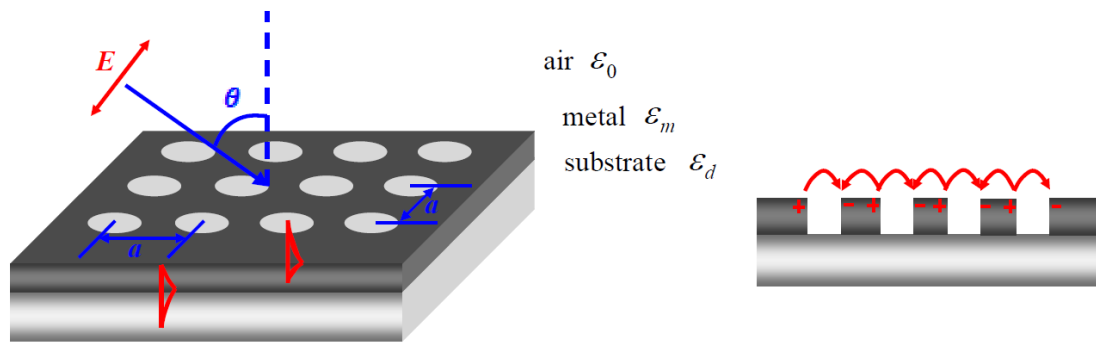


Figure 1-4 Coupling of surface plasmon through subwavelength holes by use of 2D periodic surface features. From [21].

the optical designer, as in theory it is the basis of transferring the incident light energy into a combination of discrete surface plasmon resonances. As a result of surface plasmon excitation in the metal in a subwavelength hole array structure, the light is coupled through the walls of the hole openings, to be re-radiated out the other end.

This point is what distinguishes SPP-assisted transmission from classical aperture theory: the transmitted light in the former is the result of a resonance, one which can be tailored to produce dramatic enhancements of the incident energy at specific wavelengths. Indeed, groups have reported in their surface plasmon coupling studies that, in theory, the per-hole enhancement of the incident energy is nearly unlimited [16, 44], depending on the engineering of the array within the bounds of the macroscopic Maxwell equations. That is, when each hole is considered as representing a fraction of the metal surface permitting transmission (as opposed to the fraction of the metal surface obstructing transmission), a normalization factor or “filling fraction” can be obtained which quantifies the “extraordinariness” of the transmission intensity, as compared to a standard, non-plasmonic hole.

1.3 Terahertz Plasmonics

Many studies have looked at extraordinary transmission through subwavelength apertures in the terahertz regime [19-21, 26, 29, 45-53]. Electromagnetic waves at terahertz frequencies differ from light waves in a few subtle but important ways with regards to their interaction with plasmonic hole array structures. At terahertz frequencies the imaginary component ϵ_{mI} of metal is significantly larger in magnitude than the real component ϵ_{mR} . Since $\epsilon_{mI} \gg |\epsilon_{mR}|$, the penetration of electromagnetic wave into the metal is much weaker than at optical frequencies,

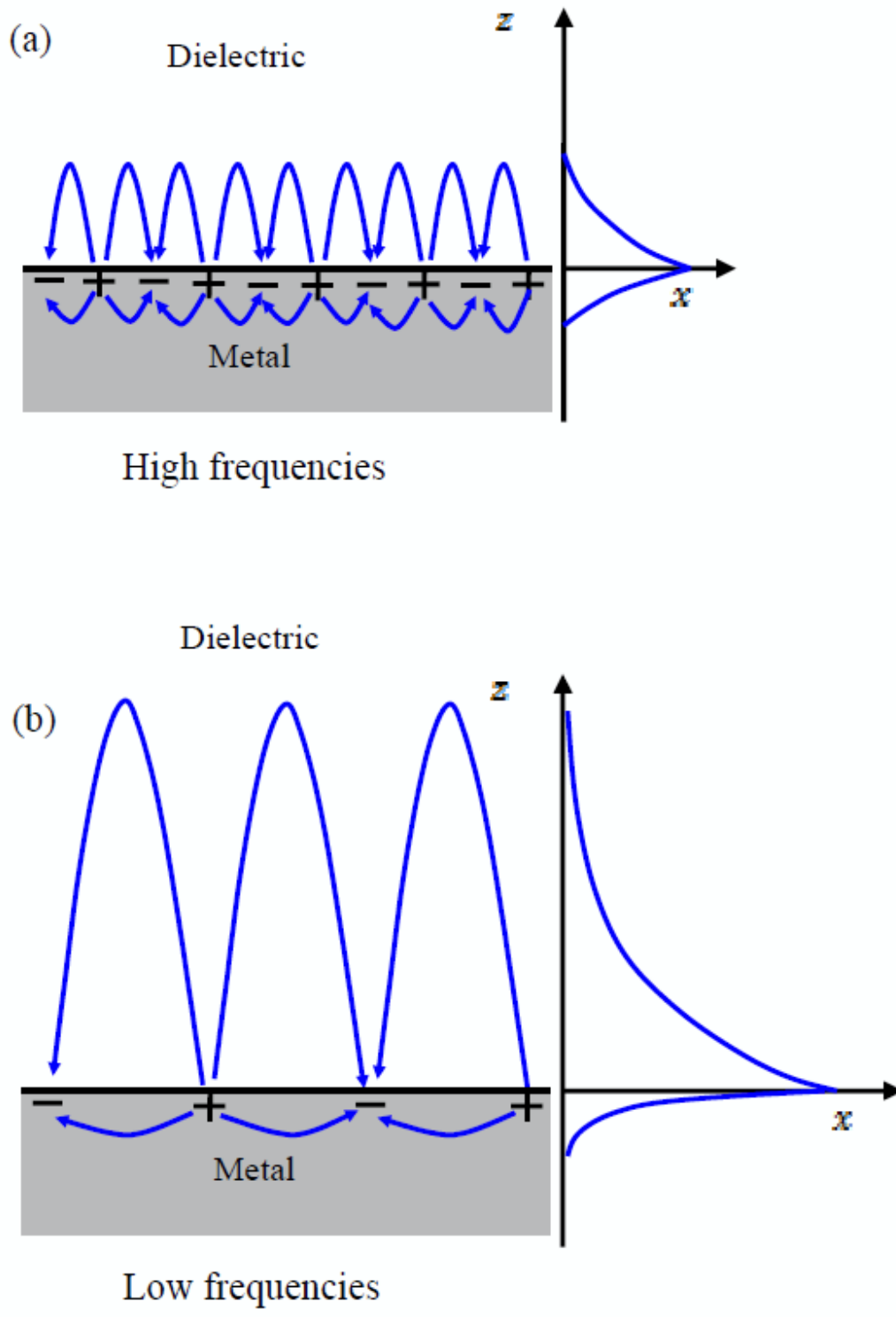


Figure 1-5 Illustration of propagation differences between optical surface plasmons (a) and terahertz surface plasmons (b). Terahertz surface plasmons exhibit lower field confinement of E_z in metal. A qualitative comparison is shown at right for the exponential decay of E_z for a surface plasmon as it propagates along the metal surface. From [21]

where $|\epsilon_{mR}| > \epsilon_{mI}$. This also corresponds to a longer propagation length, as most of the surface wave is located in the dielectric, as shown in [Figure 1-5](#).

At the interface between a metal and dielectric, ϵ_m overpowers the magnitude of ϵ_d . The consequence for Eq. (1-5) is that the zero-order SP mode \mathbf{k}_{SP}^0 at terahertz frequencies can be approximated as:

$$\mathbf{k}_{SP}^0 = \frac{\omega}{c} \sqrt{\epsilon_d} . \quad (1-6)$$

This is an interesting implication, in that it implies the Drude properties of the metal do not significantly affect the surface plasmon characteristics as is the case at optical frequencies. Therefore, generation of SPP-assisted transmission of terahertz radiation through subwavelength hole array structures is controlled largely by the surface texture. With the weak SPP field confinement, long SPP propagation length, and weak influence of ϵ_m , the surface waves generated at terahertz frequencies are more akin to Zenneck waves than SPPs [\[21, 54\]](#). It is the goal of the terahertz engineer to force the generation of these “spoof” surface plasmons to appear despite their dissimilarity to a SPP as defined by the Drude model [\[40\]](#).

The long wavelengths at terahertz frequencies (tens to hundreds of microns) are long enough compared to light waves (hundreds of nanometers) that more options are possible for the manipulation of the radiation on the subwavelength scale in a laboratory setting. Optomechanical mounts, motors, and positioners with micron precision can provide a means to obtain time-domain transmission data from terahertz subwavelength aperture experiments. Highly precise temporal signals can be measured through the use of a terahertz time-domain spectroscopy (THz-TDS) system [\[53, 55-57\]](#). This allows investigation the same varieties of effects that occur at optical frequencies, with the uniquely attractive feature of deeper insight into the time-domain propagation dynamics. An overview of the THz-TDS technique is provided in Chapter 4.

Another valuable benefit of subwavelength aperture study in the terahertz regime is that fabrication of subwavelength-scale samples can be performed easier, with less expensive equipment.

1.4 Outline of This Thesis

Chapter 2 elaborates on the main concepts introduced in Chapter 1, namely: resonances in finite-size subwavelength hole arrays modified by a periodic dielectric peg layer (DPL). The term “hole cluster” will be used in the text as a shorthand synonym for “finite-size subwavelength hole array”. The specific nature and description of the DPL structure is discussed in Chapter 3, as well as a discussion of the hole pattern design methodology, and a presentation of a finite-integration technique (FIT) model of the DPL, giving insight to its role in enhancing subwavelength hole array transmission. Chapter 4 describes the physical experiment undertaken in which a series of eleven subwavelength hole patterns were fabricated and measured using THz-TDS techniques. Chapter 5 presents the experimental results and ties the results back to the simulation discussed in Chapter 3. Chapter 6 provides a closing analysis of the study, and attempts to provide a contextual explanation of its significance in the field of nanophotonic engineering, with thrust towards future work and potential applications of DPL-modified subwavelength hole patterns and arrays.

CHAPTER II

BACKGROUND

The goal of this thesis is to study the behavior of structures composed of sets of subwavelength holes superimposed by an infinitely periodic 2D dielectric peg layer. Section 2.1 will first look at plasmonic hole and particle arrays as specialized forms of optical gratings. The common properties of both particle and hole arrays will be discussed towards understanding their common features. In Section 2.2 a discussion of subwavelength transmission through finite-size hole arrays will be presented. Special attention will be placed on the issue of how predicting and characterizing finite-size effects requires a more complex understanding of the comparatively simple grating effects discussed in Section 2.1. Section 2.3 presents an overview of findings about plasmonic resonances in periodic structures. Infinite hole array resonances, dielectric corrugation, and superlattice effects will be explained in Section 2.3.1. Section 2.3.2 will build upon the previous section with a discussion of hybridized resonances and the analogy of plasmonic oligomers as artificial molecules. The process of controlling or tailoring a hybridized resonance of this sort will be discussed in light of recent scientific findings about Fano resonances in nanostructures. All of the concepts in this section form the basic components to aid understanding the nature of the simulation and experimental results presented later in this thesis.

2.1 Surface Plasmons on Infinitely Periodic Textured Surfaces

In subwavelength hole arrays, surface plasmons are formed due to the diffraction orders set up by the hole array lattice. The frequencies of the diffraction orders are determined by the periodic surface roughness caused by the hole openings. The concept for a 1D grating is illustrated in [Figure 2-1](#). Light matching the boundary conditions at the surface of the metal will constructively interfere and form diffracted waves at frequencies predicted by the geometrically determined grating vector \mathbf{G} for a simplified, infinitely periodic 1D case:

$$\mathbf{G} = \frac{2\pi}{\Lambda}. \quad (2-1)$$

When a wave at wavevector \mathbf{k} interacts with the grating, the diffracted waves with wavevectors \mathbf{k}_m are specified as:

$$\mathbf{k}_m = \mathbf{k} + m\mathbf{G}, \quad (2-2)$$

where index m is an integer. In order to find the surface plasmons excited by the diffraction orders, the incident wave \mathbf{k} can be decomposed according to its orientation with respect to the metal surface, normal or parallel, or \mathbf{k}_\perp and \mathbf{k}_\parallel respectively. The diffracted components $\mathbf{k}_{m\parallel}$ can be expanded from \mathbf{k}_\parallel :

$$\mathbf{k}_{m\parallel} = \mathbf{k}_\parallel + m\mathbf{G}. \quad (2-3)$$

Any of the $\mathbf{k}_{m\parallel}$ that match the wavevector \mathbf{k}_{SPP} of a surface plasmon can launch a surface plasmon. As shown in Eqs. (1-5) and (1-6), the zero-order mode \mathbf{k}_{SP}^0 for a surface plasmon at a metal-dielectric interface is given by permittivities ϵ_d and ϵ_m , for the dielectric and metal, respectively. Substituting $\mathbf{k}_{m\parallel}$ in for the grating vector \mathbf{k}_R in Eq. (1-5), we can see that the

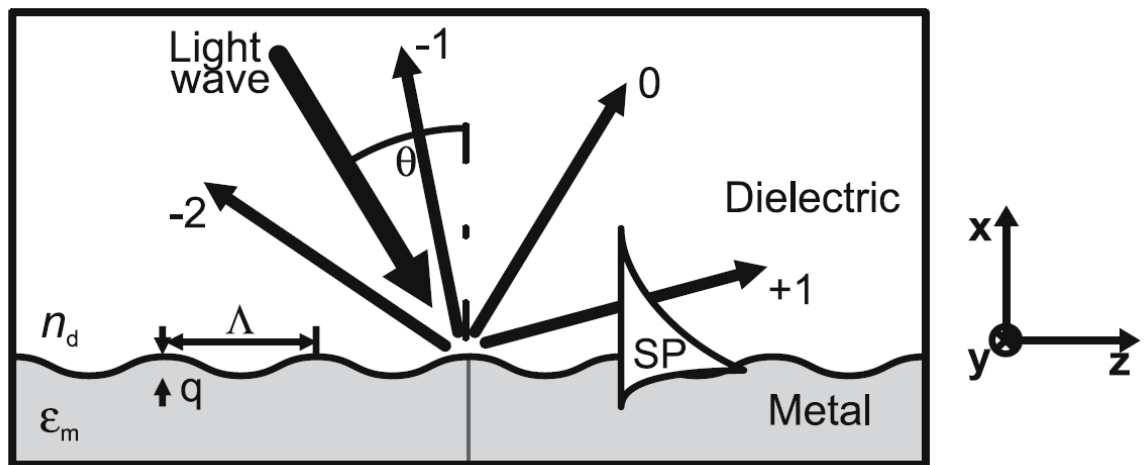


Figure 2-1 Excitation of surface plasmon due to periodic surface texture (grating) effect. In this case, the diffraction orders are determined by the depth q and period Λ of the grating. From [58].

momentum matching conditions to launch an SP can be satisfied with the diffraction orders of a grating. Therefore, the SP modes themselves form a set of orders in m .

To extend this observation for a 2D grating, we now assume two indices, m and n , for the diffraction orders. The reasoning proceeds as above for the 1D case, but includes the complexities of the 2D lattice into the diffraction order scheme rolled into the grating constant \mathbf{G}_{mn} . For a 2D square lattice:

$$\mathbf{G}_{mn} = \frac{2\pi}{L} \sqrt{m^2 + n^2}, \quad (2-4)$$

and for a hexagonal lattice:

$$\mathbf{G}_{mn} = \frac{4\pi}{\sqrt{3}L} \sqrt{m^2 + n^2 + mn}, \quad (2-5)$$

where is L the periodicity of the arrays. Correspondingly, for a 2D grating, \mathbf{k}_{SP} will now have diffraction orders in both m and n .

2.2 Transmission Through Finite-Size Subwavelength Hole Arrays

Not all subwavelength hole array devices are infinitely periodic. The attractiveness of subwavelength hole array devices is that they can squeeze light through tiny structures. The fewer holes in a structure, the more space efficient, but also, as hole number goes down, the less light that is able to be pushed through. Thus the efficiency of the enhancement process for the transmitted light in finite-size hole array devices is key. Many different hole/particle combinations have been tested in systems exhibiting infinite periodicity, but in the area of finite-size hole arrays, there are still hurdles to face, as every finite-size hole array is in and of itself

unique. Specifically, the ability to design and control the resonant properties in each finite-size hole array presents significant challenges over its infinitely periodic counterpart. The nature of this uniqueness stems from the finite number of scatterers, each of which must be taken into account for a complete characterization of the transmission.

2.2.1 Numerical Modeling of Finite-Size Hole Arrays

Identifying plasmonic effects in finite-size hole array problems via numerical analysis raises its own set of challenges. For one, the computational resources needed to model the entire problem domain can become prohibitively demanding, in contrast to modeling a unit cell of the infinitely periodic case with periodic boundary conditions. It also becomes especially challenging due to the fact that, in 3D modeling, even if finite-size hole array geometry can be broken down into 2D symmetry planes parallel to the metal film, and periodic boundary conditions imposed on them, in many non-trivial cases the perpendicular direction cannot be compacted via symmetry planes. Third, when modeling a Drude metal or other frequency-dispersive material, the metal film must either be subgridded or very densely meshed, adding more computational demands [59, 60]. A corollary to this is that if a time-domain algorithm such as FDTD is used instead of a frequency domain method, workarounds must be put in place to make the frequency-dispersive material compatible with time-varying wave equations. For FDTD, the Auxiliary Differential Equation (ADE) method, Recursive Convolution (RC) method, and the Drude Critical Points method can overcome these hurdles [61, 62], but they require subroutines that provide deviations from the procedural time-marching loops of FDTD. Again, these add computational complexity. Adding absorbing boundaries, lengthening the problem domain dimensions to account for reflections, and optimizing the mesh definition for increasing numbers of scatterers all must be taken into account to get a precise solution [60, 63-65].

2.2.2 Analytical Modeling of Finite-Size Aperture Arrays

As it has been shown in Section 2.1, the simplified unit-cell grating theory has no easy way of predicting the field enhancement due to a finite-size collection of scatterers. In fact, outside of numerical simulation, the theoretical framework required to describe finite-size processes is significantly more involved. Even though larger and larger finite-size hole arrays might appear to approach the idealized solution for an infinite array of holes, the difference in the problem setup between the two cases makes all the difference in the world. In this section, an analytical method is discussed which is capable of treating both finite-size and infinite systems equally well.

It was shown by [66] that the effects seen in 2D periodic arrays of subwavelength holes can also be observed in a 1D chain of subwavelength holes. To explain the plasmonic phenomena in these special types of structures, the same group developed modal formalism which extended equally well to descriptions of finite-size 1D chains, and both infinite and finite-size 2D arrays of holes, for arbitrary illumination [4, 44, 66].

The equations for the modal expansion are derived completely in [4, 16], and are summarized here. First, they assume a thin metallic layer containing up to thousands of scatterers, in any arrangement, which can be either holes or “dimples” (indentations). All that needs to be defined about each of these scatterers is the propagation constants for the waveguide modes supported within the hole. If all of the scatterers in the film are identical in shape, then the problem is simplified quite a bit. For an infinite hole array, all of the possible waveguide modes native to each of the holes in a unit cell are expanded separately into their plane wave components, which emanate from their respective hole openings. The set of all of these waveguide modes in the hole array structure is referred to as the index α . The momentum matching condition for the surface

plasmon scattering is a result of inclusion of surface impedance boundary conditions (SIBCs) for the metal film in the expression:

$$| \mathbf{E}' \rangle = \sum_{\mathbf{k}_{\parallel}\sigma} t_{\mathbf{k}_{\parallel}\sigma} e^{ik'_z(z-h)} | \mathbf{k}_{\parallel}\sigma \rangle , \quad (2-6)$$

where \mathbf{E}' is the transmitted electric field, $\mathbf{k}_{\parallel}\sigma$ are the parallel \mathbf{k} vectors at polarization or σ (s polarizations) arising from the plane wave expansions of the waveguide modes at the hole openings, h is the metal thickness, and $t_{\mathbf{k}_{\parallel}\sigma}$ represents the transmission coefficient associated with each $\mathbf{k}_{\parallel}\sigma$. The quantity $t_{\mathbf{k}_{\parallel}\sigma}$ is given by

$$t_{\mathbf{k}_{\parallel}\sigma} = -\frac{1}{f'_{\mathbf{k}_{\parallel}\sigma}} \sum_{\alpha} \langle \mathbf{k}_{\parallel}\sigma | \alpha \rangle E'_{\alpha} , \quad (2-7)$$

where E'_{α} represents the electromagnetic waves formed by each member of α for the hole openings on the transmission side of the film. The quantity $f'_{\mathbf{k}_{\parallel}\sigma}$ contains the SIBC information:

$$f'_{\mathbf{k}_{\parallel}\sigma} = 1 + z_s Y_{\alpha} , \quad (2-8)$$

where

$$z_s = \frac{1}{\sqrt{\epsilon_M}} , \quad (2-9)$$

and ϵ_M is the dielectric constant of the metal material, and z_s relates the electric field to the magnetic field by:

$$\mathbf{E} = z_s \mathbf{H} \times \mathbf{u}_n , \quad (2-10)$$

where \mathbf{u}_n is the unit vector normal to the metal surface and pointing into its interior. The quantity Y_{α} represents the admittances of the TE and TM modes for each α .

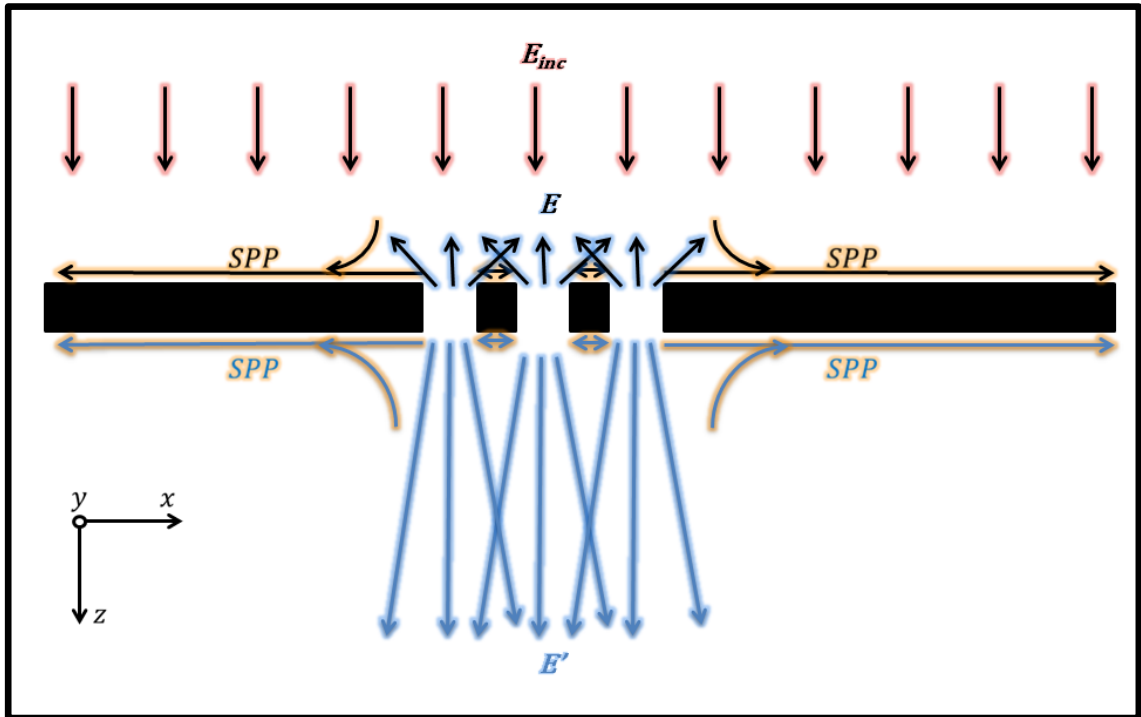


Figure 2-2 Schematic for light scattering in a finite-size plasmonic hole array illuminated by a uniform plane wave (E_{inc}). Light can scatter between holes on the incident side (E) or the transmitted side (E') via waves or surface plasmon polaritons (SPPs).

To find the transmitted fields everywhere in space from the E'_α , the term $t_{k\parallel\sigma}$ is found via the discrete sum over all α in Eq. (2-7). To relate this back to the incident illumination of the array, a set of coupled equations exist:

$$(G_{\alpha\alpha} - \Sigma_\alpha)E_\alpha + \sum_{\beta \neq \alpha} G_{\alpha\beta}E_\beta - G_\alpha^V E'_\alpha = I_\alpha , \quad (2-11)$$

$$(G'_{\gamma\gamma} - \Sigma_\gamma)E'_\gamma + \sum_{\nu \neq \gamma} G'_{\gamma\nu}E'_\nu - G_\gamma^V E_\gamma = 0 , \quad (2-12)$$

which relate the behavior of the entire system on the incident and transmitted sides. Eqs. (2-11) and (2-12) function in tandem, where Eq. (2-11) deals with the illumination I_α on the incident side and Eq. (2-12) deals with the transmitted side, where indices α , β , γ , and ν are indices for the hole modes on the incident (α and β) and transmitted (γ and ν) sides. The β quantity represents the exact same waveguide modes as found in α and is needed so the math can be computed in matrix form and therefore simultaneously take into account every possible scattering action between every possible hole mode. The indices γ and ν on the transmitted side are identical in function to α and β , but take into account the material properties on the transmitted side (e.g. the substrate the metal film rests upon). All G terms are related to coupling events, either hole to hole ($G_{\alpha\beta}$ and $G'_{\gamma\nu}$) or hole entrance to hole exit (G_α^V and G_γ^V). The terms Σ_α and Σ_γ are related to the multiple reflections within the hole between the entrance and exit.

The point where the formalism intersects for both infinite and finite-size systems comes with definition of the key coupling coefficient $G_{\alpha\beta}$. For an infinite hole array, $G_{\alpha\beta}$ is given by the discrete sum:

$$G_{\alpha\beta} = \sum_{k\parallel\sigma} \frac{Y_{k\parallel\sigma}}{Z_{k\parallel\sigma}^+} \langle \alpha | \kappa \rangle \langle \kappa | \beta \rangle , \quad (2-13)$$

where κ are the diffraction orders for the given unit cell of length L_x and width L_y . For a finite-size array, the discrete sum over diffraction orders in Eq. (2-13) is replaced by integration over the diffraction orders $\mathbf{k}_{\parallel\sigma}$. This is due to the fact that now the unit cell is effectively infinite in size. As $G_{\alpha\beta}$ describes the ability of the holes to couple light from the incident side to the transmitted side, it is the key quantity for which to be solved.

The surface plasmon effect is taken into account from the SIBCs imposed in Eq. (2-7). If a PEC conductor is assumed in the SIBCs by setting $z_s = 0$ (as would be a reasonable approximation at terahertz frequencies), the equations are simplified. For surface plasmons at terahertz frequencies, the PEC approximation in this formalism functions analogously to the weak field confinement effects discussed in Chapter 1.

2.3 Resonances in Subwavelength Hole Arrays

2.3.1 Lattice and Superlattice Resonances

An early study [67] found that the rotational symmetry of their hole arrays had a direct effect on the subwavelength transmission enhancement, while keeping the lattice constant the same in each of the different types of hole arrays. They found that hexagonal lattices allow superior transmission enhancement over lattices exhibiting square or “graphite” rotational symmetries. Hole opening shape has been shown to play a critical role [21, 50, 68], especially the length/width ratio of elliptical and rectangular holes [21, 50], and that varying these dimensions alone can allow tuning of the surface plasmons bound to the metal surface [68]. This effect can be explained by a combination of surface plasmon SPP and localized surface plasmons LSPs. LSPs are formed around the rectangular holes due to the subwavelength geometry. The same LSP

effects occur at the surfaces of isolated metallic nanoparticles, for instance. Controlling the mixture of the grating-type SPP and the LSP component is a subject of much interest in nanophotonic engineering.

It has been shown that using a periodic dielectric layer on the surface of a subwavelength structured metal film could enhance the transmission and absorption effects of the system, and allow opportunities to tune the plasmonic resonance [69]. It has also been shown that a periodic layer of dielectric bars above the surface of single subwavelength slit enhances the transmission of light through the structure [31, 70]. The dielectric bars are able to boost the composition of k_R for surface plasmon coupling at certain frequencies. Other types of dielectric corrugation include 2D lattices. Glass nanopillars inserted into subwavelength hole arrays have been shown to enhance transmission of the hole arrays, and to alter the transmission spectrum due to what could be described as a hole-widening effect [71-74]. Though the posts do not change the lattice structure of the holes, they do not in and of themselves change the SPP frequency, but as they increase the index of refraction in the vicinity of the hole, they help to confine more of the incident light above the hole opening. Another analogy is that of an array of dielectric antennas. The periodic pillars are oriented in the same direction of the electric field of the surface plasmon, which itself is a transverse magnetic (TM) wave. By superposition, TM modes formed by the dielectric pillar lattice can add to the surface plasmons launched by the hole lattice. Another way to explain the origin of the effect is to look at it from a “grating” perspective, wherein the surface corrugation of the hole array itself is effectively enhanced, as the surface is made “rougher” by the addition of the semi-transparent surface features. Another effect of dielectric corrugation is better control of the beaming of light transmitted out of the hole array, without having to significantly alter the surface plasmon resonance frequency.

One fascinating dimension to plasmonic gratings is the nature of the results reported for nested plasmonic lattices and plasmonic superlattices. The theory behind these gratings is that on one level there exists a hole or particle grating of a certain periodicity, which in itself is part of a meta-array of identical hole gratings. One study of gold particles of varying heights fabricated above the openings of a plasmonic hole array shows that varying the particle height enhances the transmission of light through the hole arrays by means of localizing the optical fields around the nanoparticles, and hence suppressing the radiative decay of the SPP field [75]. A study of a series of finite-size hole arrays superimposed by an infinite hole array layer of the same period showed that by varying the physical separation distance between the two layers, new resonances could be induced in the transmission spectrum [76], due evidently to new resonances inherent to the combined “superlattice”.

2.3.2 Plasmonic Oligomers, Hybridized Plasmons, and Fano Effects

Studies on plasmonic nanowires show that stacking them in superlattice structures causes “hybridization” of surface plasmons [77, 78]. The concept of hybridization of surface plasmon resonances is explained elegantly in the analogy of light interacting with a molecule. When light energy is incident on a molecule system, it is subject to the resonances it will encounter in the structure, which in a simplified manner of speaking can be categorized as modes inherent to either molecular orbitals or atomic orbitals. The molecular orbitals have unique collective electronic effects arising from the dynamics of the shared electrons in the system. The atomic orbitals derive their own unique electronic effects due to charge interaction between the nucleus of the atom and its associated electron clouds. An depiction of the molecular-type resonances calculated by [79] for a plasmonic trimer is shown in Figure 2-3.



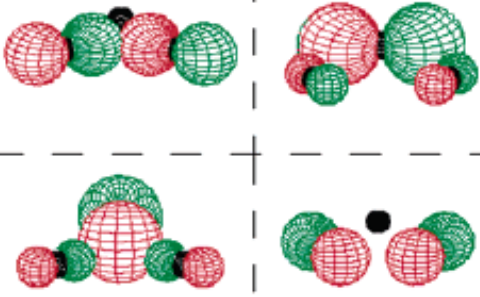

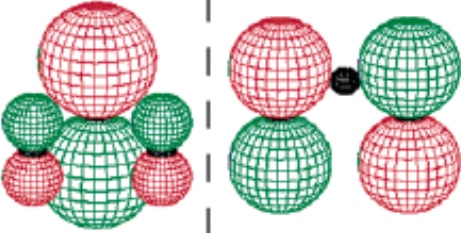
Irreducible representation	Visualization (side)
A_1'	
A_2'	
$2E'$	
A_2''	
E''	

Figure 2-3 Diagram of the possible dipolar resonances in a plasmonic trimer, calculated using group theory. Plasmonic hybridization occurs due to excitation of surface plasmons from the collective “molecular” dipoles seen above, and the surface plasmons from the “atomic” dipoles due to the shape and material composition of the three nanoparticles. From [79].

To extend this explanation to a finite-size hole array, we will consider an infinitely hexagonal array of periodic subwavelength holes, which has been broken down into the small system of only 37 holes shown below in [Figure 2-4](#). From the plasmonic hybridization standpoint, the light interacting with this 37-atom artificial molecule then has the potential to express the resonances of the grating interferences (atoms) and the unique resonances scattered by the dipole possibilities in the superstructure (molecule). The atomic resonances are already explained via infinite grating theory as in Eqs. (2-1)-(2-5), and the molecular type resonances can be deduced from a more rigorous theoretical formalism like the one introduced in Eqs. (2-6)-(2-13).

This particular intersection between infinite grating resonances and finite-size resonances falls under the category of Fano effects. The Fano effect is named after Ugo Fano, whose widely influential work on coupled harmonic oscillators [80] explains asymmetric resonances peaks as the result of a coupling between a strong, discrete resonance and a slowly varying “nonresonant” continuum. The degree of asymmetry of the resonance can be quantified by q_ν in the formula for the Fano lineshape:

$$T_{fano}(\omega) = |t(\omega)|^2 = T_a + T_b \frac{(\varepsilon_\nu + q_\nu)^2}{(1 + \varepsilon_\nu^2)}, \quad (\text{Eq 20})$$

where T_a is the slowly-varying continuum, T_b is the zero-order discrete state, and ε_ν is a placeholder to relate the Fano profile to subwavelength hole array transmission:

$$\varepsilon_\nu = \frac{\omega - \omega_\nu}{\Gamma_\nu/2}, \quad (\text{Eq 21})$$

where ω is angular frequency, ω_ν is the resonance frequency, and Γ_ν is the linewidth. The asymmetry parameter q_ν gives an idea of the strength of coupling between the T_a and T_b states [21]. Another way of looking it is by simply viewing the Fano lineshape as the superposition of

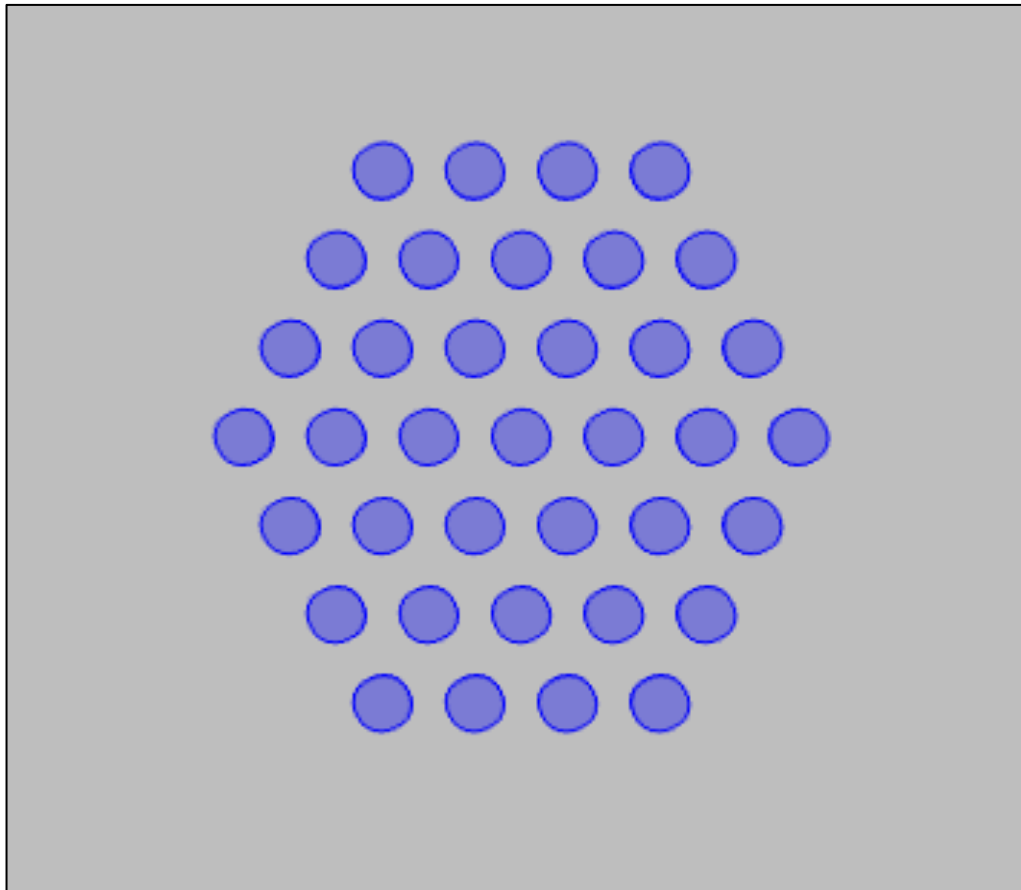


Figure 2-4 Finite-size array of 37 holes in metal film.

two resonances, one strong and narrow, and one “dark” resonance with a broad linewidth and its own separate resonant frequency, as seen in the frequency response of an electric circuit composed of two inductively-coupled RLC networks [81].

Recent research has provoked much interest in the Fano resonance. Numerous studies in plasmonic oligomer structures point out the benefits of manipulating the Fano resonance in nanoscale objects to tailor the resonance peaks of the system’s response to light [17, 35, 36, 51, 82-86]. For instance, one group studying plasmonic hexamer groups has shown that by inserting or removing an extra particle inside the hexamer [85], the resonance peak location can be “switched”. The inserted particle itself can be varied in shape to tune the switched resonance in finer detail [36]. The Fano effect has been observed in geometries of rings of nanoparticle “necklaces” [24], oligomers of various numbers of particles [17, 35, 78, 83-85, 87], oligomers using asymmetric particles, and hybrid oligomers formed by (Figure 2-5) inserting and removing dielectric particles in select locations to modify the “molecular”-type collective resonances of the system in order to “transmute” the surface plasmons in the structure [86].

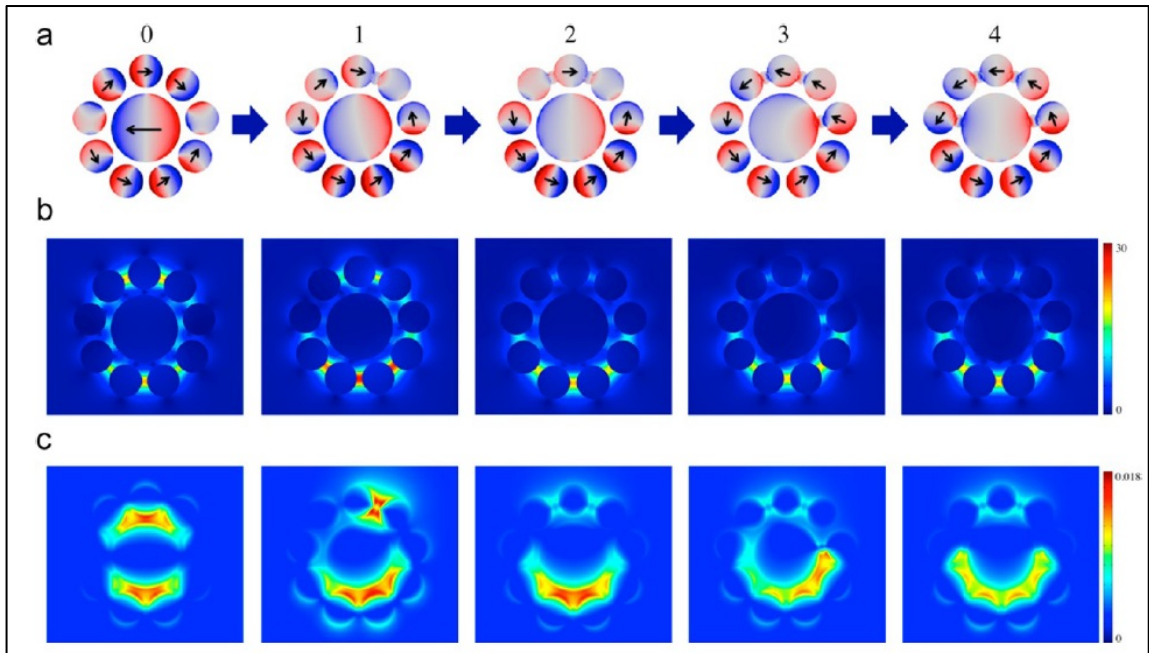


Figure 2-5 Tuning a Fano resonance by inserting small dielectric particles into a plasmonic decamer of gold nanoparticles. The number at the top of each diagram refers to the number of small dielectric particles inserted into the structure. The center and bottom rows show the simulated electric and magnetic field distributions, respectively at the resonant frequency [86].

CHAPTER III

DESIGN AND SIMULATION OF PLASMONIC HETEROSTRUCTURES

This section describes the methodology used to design the hole cluster heterostructures. Section 3.1 and its subsections describe the issues unique to designing the finite-size hole cluster heterostructures in this study. Subtle differences in design approach were taken in the design of the “h”, “r”, and “rand” configurations, and those specific details are discussed in sections 3.1.1, 3.1.2, and 3.1.3, respectively. Section 3.2 describes the modeling process for an infinitely periodic hole array with a DPL as a proof-of-concept exercise to compare with and validate the experimental results. Section 3.2.1 describes the results of the simulation with regard to the fundamental resonance enhancement observed at 0.58 THz. Section 3.2.2 looks at the reflection spectra and surface current plots obtained from the simulation to provide a brief discussion of the transmission peaks observed at the higher frequencies.

3.1 Design Considerations

The overarching goal of the structure design process was to create a series of experimental samples to test various capabilities of a DPL consisting of short cylinders positioned inside the holes in a subwavelength hole array. The cylindrical peg would be inset into the cylindrical holes and rest on the silicon substrate, with the bulk of the peg jutting out above the surface of the metal (Figure 3-1a). As viewed from above, the layer geometry would look similar to a hexagonally periodic array of tree trunks. Since a small bit of each peg fit snugly into its corresponding hole,

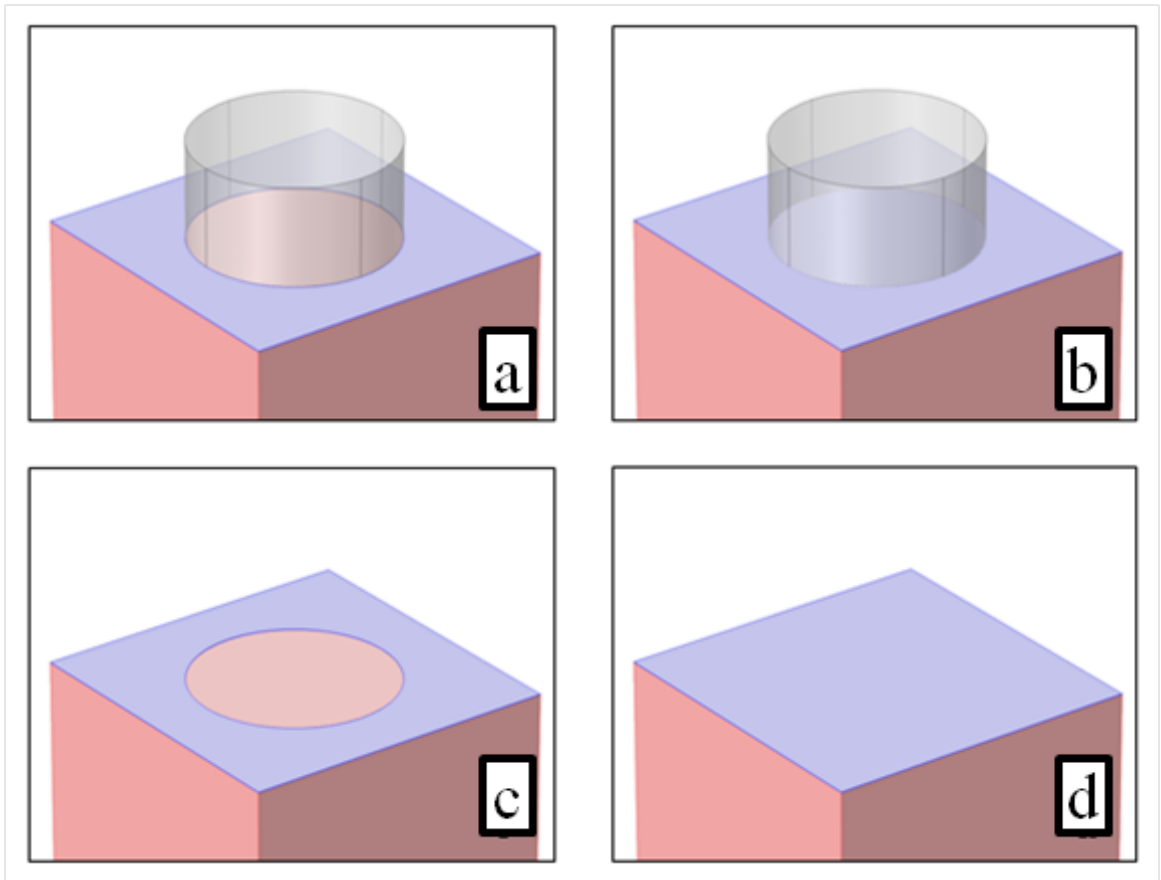


Figure 3-1 Each plasmonic heterostructure investigated in this study was composed of a thin aluminum film perforated with a cluster of subwavelength holes exhibiting hexagonal periodicity. Terahertz transmission of each hole cluster was measured both with and without a dielectric peg layer (DPL). Design of the plasmonic heterostructure allowed for the following four combinations of metal film (blue), substrate (red), or dielectric peg (translucent): (a) DPL, hole underneath peg (b) DPL, no hole underneath peg (c) bare metal, with hole. (d) bare metal, no hole.

with the bulk of the height of the peg sticking out into the surrounding air, the DPL moniker was chosen to conceptually characterize the geometry. If the hole array pattern was designed such that no hole was present beneath a peg, the peg would simply rest on the flat metal surface (Figure 3-1b).

The hypothesized effect of the DPL would be to enhance the surface roughness of the hole array, thereby boosting the amount of radiation coupled through the holes. Posed as an engineering design question: Is there a way to mitigate the loss of energy transmission due to “missing” holes without significantly affecting the value of the resonance frequency of the plasmonic structure? And, if so, would this effect be applicable to different geometrical arrangements of holes more so than others?

Finite-size hole arrays, in the form of ordered clusters, were chosen so that transmission through the DPL could be studied in multiple hole arrangements based on the same underlying lattice constant. The lattice constant $a = 160 \mu m$ was chosen primarily so that aspects of the transmission spectrum could be compared to already-published findings on infinitely periodic subwavelength hole arrays at terahertz frequencies [19, 21, 50]. Circular holes were chosen so as to minimize any localized surface plasmons that may be caused by unwanted asymmetry of the aperture cross section, as well to prevent different small variations in the positions of the samples in the beam path from introducing unwanted polarization effects in the transmitted radiation [5, 19-21, 50]. A depiction of an example plasmonic heterostructure is shown in Figures 3-2 and 3-3, for the case without and with a DPL, respectively. The sample in Figure 3-3 is shown again in Figure 3-4 but rendered in a slightly different color scheme, in order to highlight the surface corrugation of the DPL.

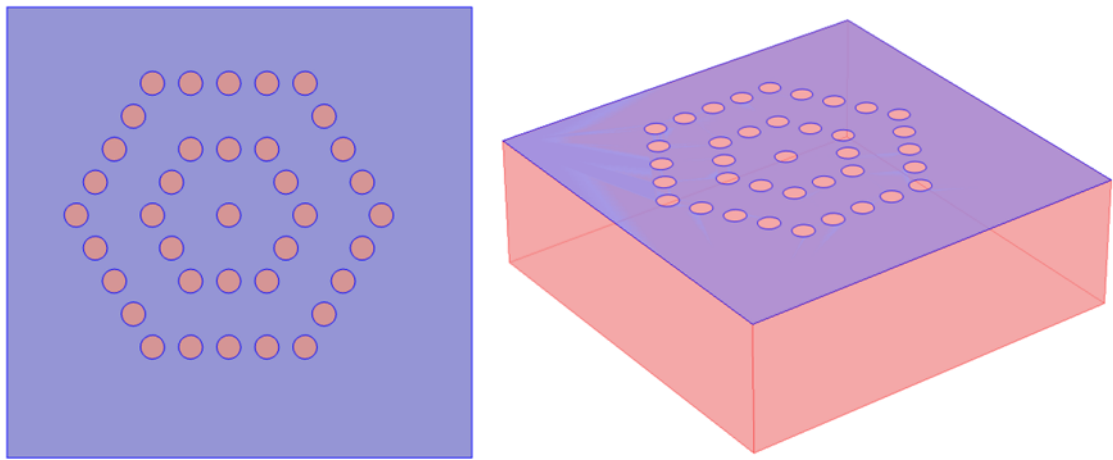


Figure 3-2 Left: Example 2D layout of a subwavelength hole cluster. The arrangement of the holes in the cluster is based on positions in an infinitely periodic array of holes with lattice constant of $160\ \mu\text{m}$ and hexagonal rotational symmetry. Red regions indicate hole openings, and purple region represents the metal film. Nearest neighbor hole distance is $160\ \mu\text{m}$, hole radius is $50\ \mu\text{m}$. Right: To-scale 3D depiction of bare aluminum hole cluster layer (purple) on silicon substrate. Aluminum film thickness is $350\ \text{nm}$, silicon substrate thickness is $640\ \mu\text{m}$.

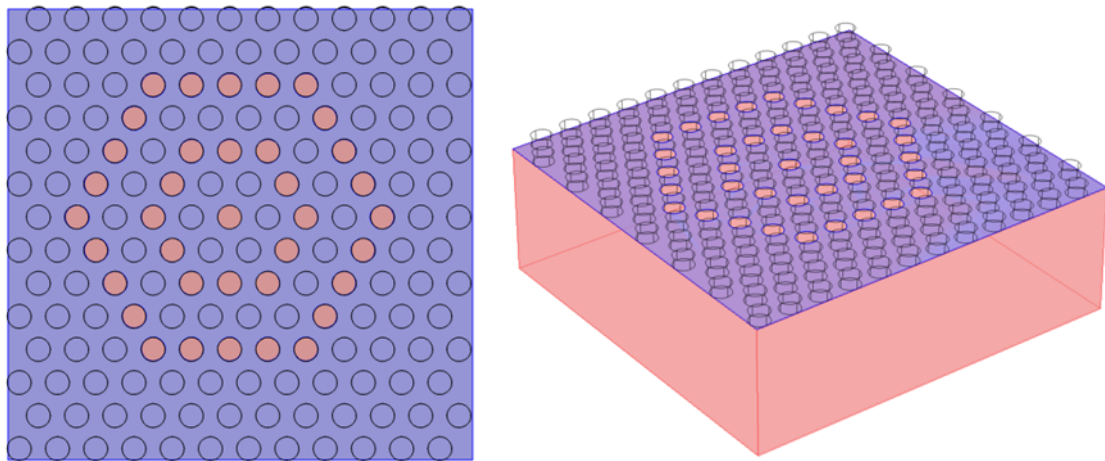


Figure 3-3 Left: Bird's eye view layout of an example subwavelength hole cluster, showing the positions of the subwavelength holes in the DPL. The arrangement of the holes in the cluster is based on positions in an infinitely periodic array of holes with lattice constant of $160\ \mu\text{m}$ and hexagonal periodicity. Red regions indicate location of holes. Periodically arranged dielectric pegs are positioned everywhere on the surface of the metal layer, and rest on top of each of the hole openings. **Right:** To-scale 3D depiction of hole cluster with DPL. Dielectric pegs are rendered as transparent wireframe objects.

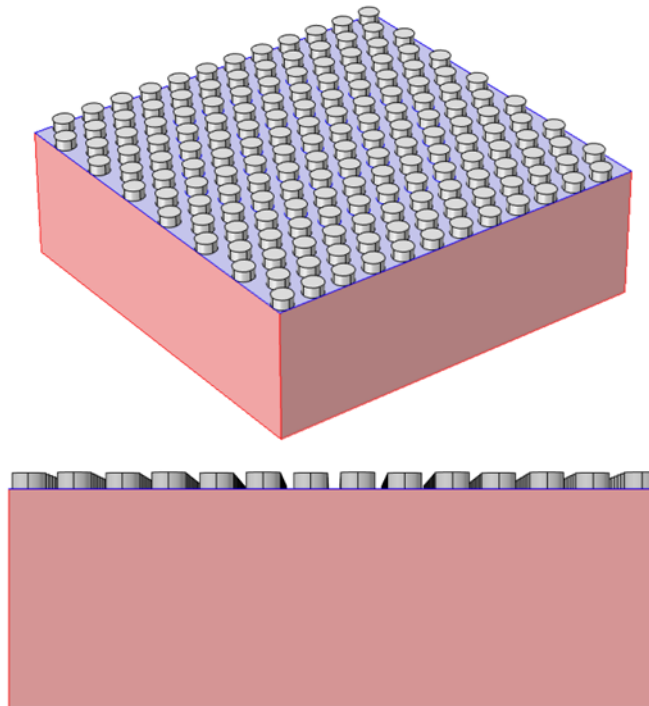


Figure 3-4 To-scale 3D views of plasmonic heterostructure design shown in [Figure 3-3](#). The dielectric pegs in this figure are rendered opaque, to show the surface texture of the DPL.

Studies have reported extraordinary transmission in hole arrays containing as few as 10 holes [52]. As number of holes increases, finite-size effects become less apparent, and the unit-cell model of an infinitely periodic array becomes more accurate [4, 16, 44, 66, 88]. On the one hand, fewer holes in a plasmonic hole array means less light-harvesting ability of finite-size subwavelength hole array structure, but on the other hand, if the transmission enhancement properties of the infinitely periodic counterpart of the finite-size array can be preserved (namely, the shape and location of the peak in the transmission response), it might actually be beneficial to minimize the number of holes in certain plasmonic devices. For instance, in nanofabricated optical semiconductor device chips [8, 9], where spatial “real-estate” needs to be carefully conserved, the reduction of the amount of holes in a plasmonic sub-component device allows more room for other sub-components on the same chip. In hopes of observing such an effect, a series of hole arrays was designed. Each sample contained a unique pattern of circular holes in an aluminum film, with the number of holes in the pattern varying from 7 to 127. The significance of each pattern design will be discussed in sections 3.1.2, 3.1.3, and 3.1.4.

3.1.1 Design of “h” Clusters

Five of the samples tested in the study contained hole clusters in “h” configuration. The h7, h19, h37, h91, and h127 patterns contained finite-size arrays of 7, 19, 37, 91, and 127 holes, respectively (See Figure 3-5). The samples were spaced with hexagonal periodicity, with lattice constant $a = 160 \mu m$ and hole radius $r = 50 \mu m$. The outer perimeter of each “h” cluster was hexagonal in shape.

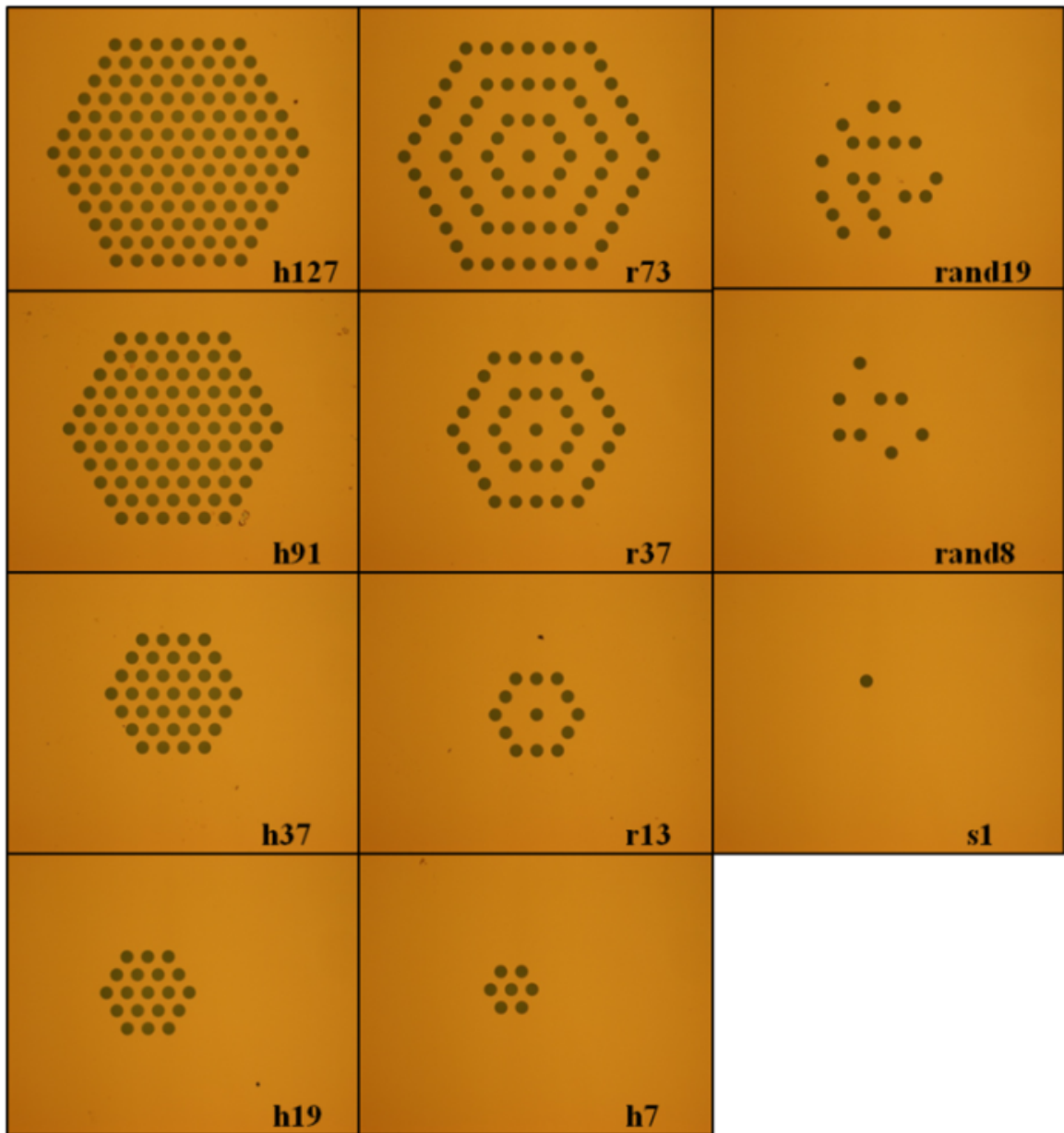


Figure 3-5 Microscope images of the mask patterns used for photolithographic fabrication of the hole clusters used in the experiment. Labeling convention is as follows: "h" stands for hexagonally periodic clusters. "r" stands for ring clusters. "rand" represents disorganized or "random" clusters. "s" stands for "single hole". The numbers in each label indicate the number of holes in each cluster.

3.1.2 Design of “r” Clusters

The r13, r37, and r73 cluster design consisted of subwavelength holes grouped in concentric rings. Each hole was positioned on select locations on an infinitely periodic hexagonal lattice, as shown in [Figure 3-3](#). The design philosophy behind these structures was identical to the “h” clusters, except that the holes in “r” are more loosely distributed. That is, the filling fraction of these arrays is smaller, where the filling fraction is defined as the ratio of the surface area of the hole openings to the surface area of the metal film. The method used to define the filling fraction for the finite-size hole clusters in this study was the same as used in a previous finite-size subwavelength hole array study [52] where the researchers normalized the measured transmission spectra by the so-called “porosity” P of the structure. Porosity, is defined here as the proportion of hole area to the aperture area, where the aperture area is defined as the area of a circle with the minimum diameter required to completely enclose all holes in the array. P is used in the data analysis in this study as a normalization constant to quantify the extraordinary transmission of different structures with subwavelength holes, allowing a standard of comparison of the transmission efficiency of each hole cluster. Using the normalization constant P also allows comparison of the relative effects of the DPL on arrays with the same aperture area yet differing numbers of holes. The method for obtaining the P value for a given pattern is shown in the diagram in [Figure 3-6](#).

3.1.3 Design of “rand” Clusters

The “h” and “r” clusters were designed as radially symmetric patterns located as select points on an infinite, hexagonally periodic lattice. The two “rand” samples exhibited no such radial symmetry because they were designed to test the ability of the DPL to enhance the transmission of “disordered” hole clusters. In other words, these structures were designed to find out if

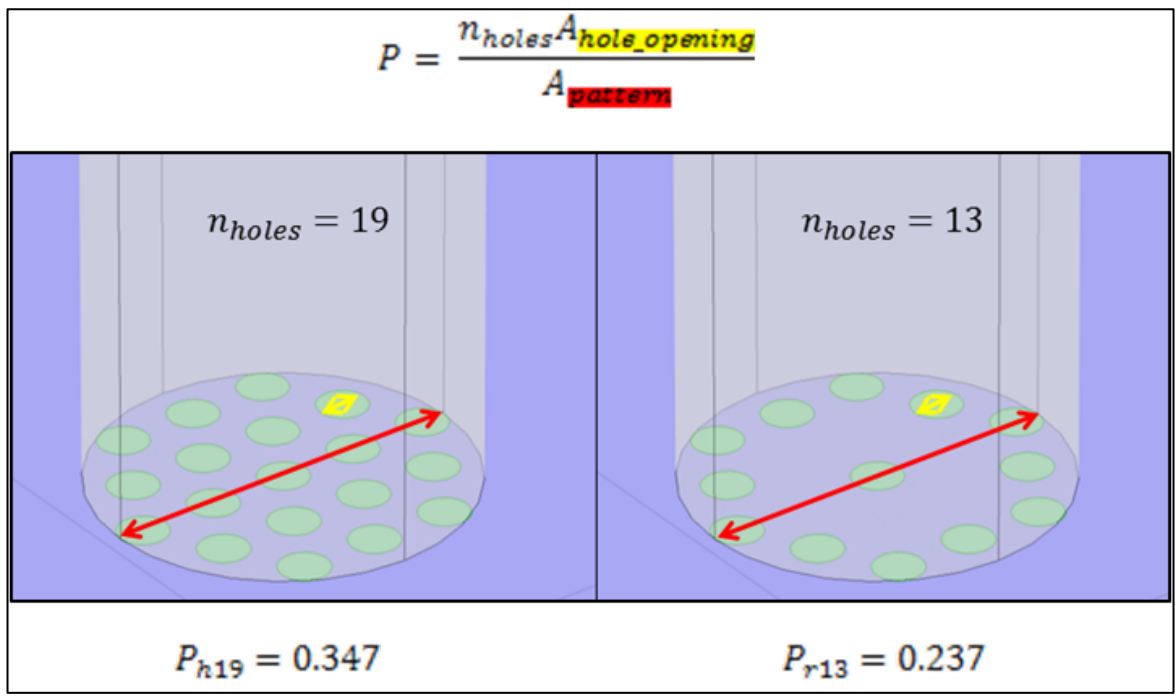


Figure 3-6 Quantitative method for obtaining normalization constant P for hole cluster porosity for two example structures: h19 (left) and r13(right).

transmission enhancement could occur in hole clusters that exhibit weak surface plasmon coupling at the fundamental resonance otherwise seen in periodic hole arrays. In analyzing the transmission properties of the “rand” structures, this study did not seek to assign a porosity value to the hole distribution, due to the strong asymmetry of the pattern. To assess the DPL effect, the transmission spectra was compared before and after the DPL was fabricated on the bare metal hole cluster layer. A final sample was constructed containing only one hole. In the end, this structure was used to assess the noise floor of the measurement system. The patterns for the rand8 and rand19 samples are shown in [Figure 3-5](#).

3.2 Modeling the DPL Effect

Simulated time-domain analysis was performed using the CST Microwave Studio (CST MWS) design tool. CST MWS uses the Finite Integration Technique (FIT) to solve electromagnetic problems, and was well-suited for modeling the transmission properties of an infinitely periodic array of hexagonally spaced subwavelength holes. The model was constructed from a unit cell with periodic boundary conditions imposed by PEC and PMC side walls. The size of the simulation domain was reduced by exploiting the 2D symmetry planes in the x and y directions, as shown in [Figure 3-7](#). The simulation was discretized using the hexahedral mesh auto-generated by CST MWS. For the transmission plots, the S21 (transmission) and S11 (reflection) parameters were solved for assuming an ultrafast input pulse whose Fourier transform spanned 0.2-2.5 THz. The S21 transmission data was normalized to the filling fraction of the hole array.

The metal film was modeled as a perforated PEC sheet having a thickness of 2 μm . The metal film thickness was chosen to be thicker than the 350 nm-thick aluminum layers in the experimental structures measured in the lab. The expanding of the metal thickness cut back

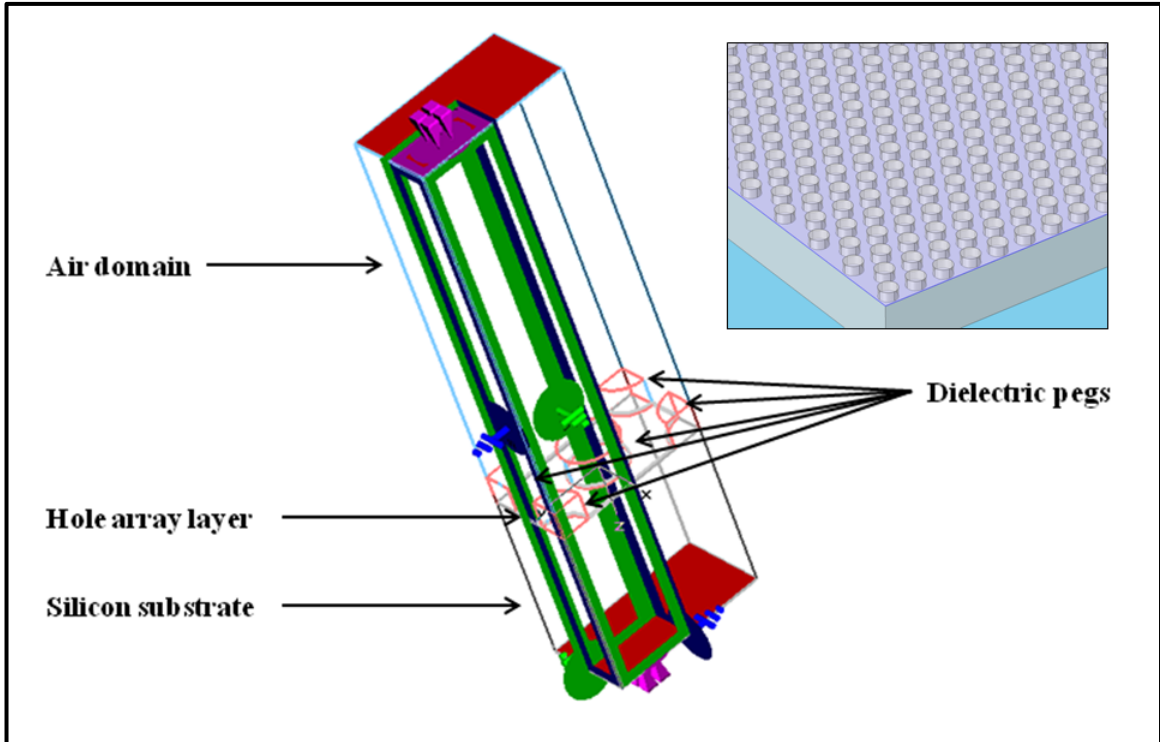


Figure 3-7 Boundary conditions for unit cell of simulation. PEC walls are in x direction, PMC walls are in y direction. Symmetry planes are exploited in unit cell to reduce computational domain size. On top and bottom port are CPML absorbing BCs. Inset: Macro-scale infinitely periodic hole array and DPL heterostructure.

computational strains on the CST MWS solver by allowing a coarser mesh inside the material. The film was modeled both using the Drude parameters for aluminum and the PEC approximation, with no significant differences in the results. This finding is substantiated by the fact that in practice, electromagnetic SPs in subwavelength hole arrays exhibit low field confinement in metals at THz frequencies [47, 89, 90]. Therefore, a PEC film was chosen as an approximation of aluminum in the simulations. All of the simulated results in this study are modeled using a PEC film.

3.2.1 Enhancement of the Main Resonance

Dielectric pegs were modeled to be identical in size and shape to the experimental structures, with radius of 50 μm and a height of 50 μm . The dielectric constant of the pegs was varied in several simulations to show the effect of the peg material on transmission. The results for S21 are shown in Figure 3-8. All the simulated spectra show a resonance peak near 0.57 THz, which is consistent with the range of experimental results reported in a previous similar experiment using subwavelength rectangular holes spaced on a hexagonal lattice with a periodicity of 160 μm [50]. The deviation from the predicted $[\pm 1, 0]$ metal-silicon surface plasmon resonance of 0.63 THz was explained in [50] as resulting from a combination between resonant and nonresonant transmission, whereas the predicted value of 0.63 THz only takes resonant component into account. The role of resonant and nonresonant contributions will be revisited and explained in greater detail in the Chapter 5, where the observed asymmetry becomes even more pronounced in the experimentally obtained transmission spectra of the finite-size hole arrays.

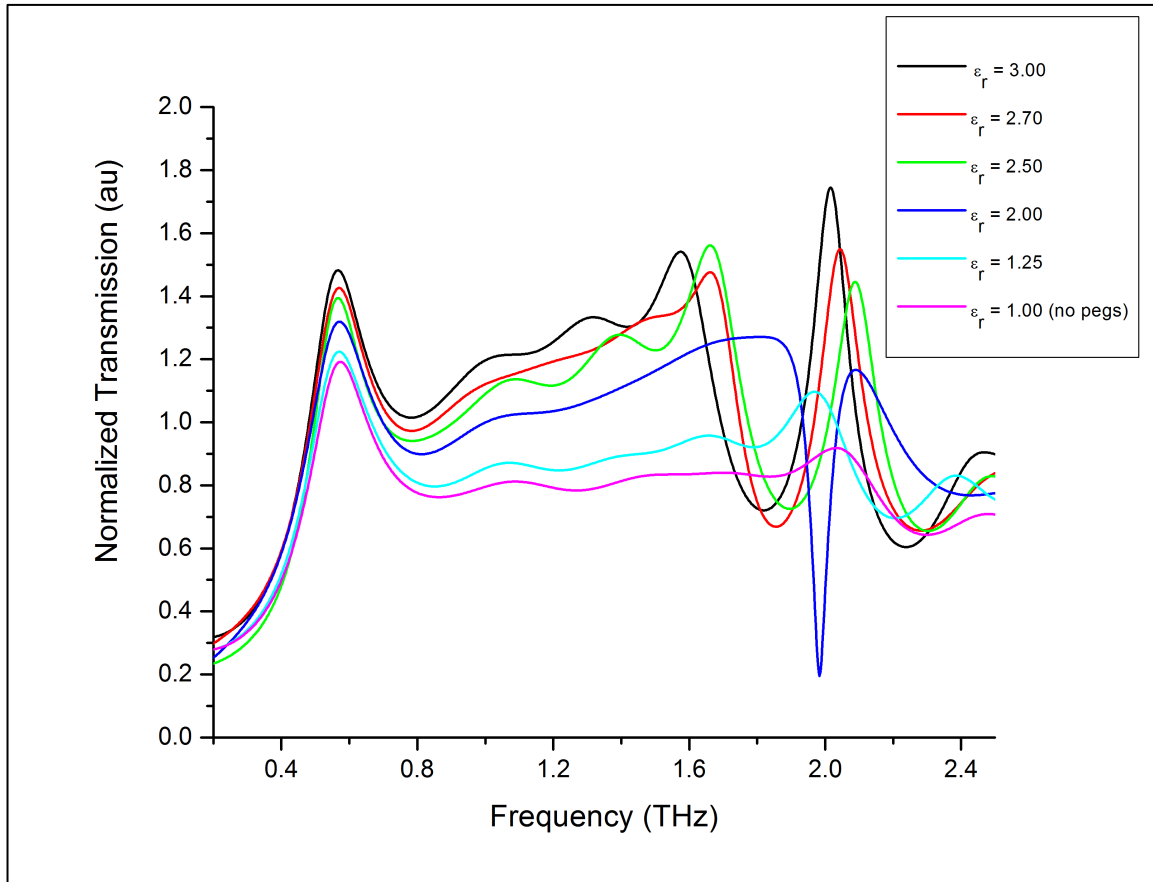


Figure 3-8 Simulated normalized transmission spectra for infinite hole array with DPL. The dielectric constant of the pegs is varied from $\epsilon_r = 1.00$ (no pegs) to $\epsilon_r = 3.00$.

The S21 plots show an increase in transmission of the fundamental transmission peak with increasing dielectric constant ϵ_r of the dielectric pegs. The plot corresponding to $\epsilon_r = 2.70$ represents the dielectric constant of the negative photoresist material used in the dielectric pegs of the experimental section of this study. The dielectric constant increase from 1.00 (air) to 2.70 (negative photoresist) corresponds to a 19.7% increase in transmission at the fundamental resonance and a very slight red shift in resonance frequency from 0.575 to 0.570 THz.

Figure 3-9 shows the field distribution plots for the z-component of the electric field at 0.58 THz for both the non-DPL and DPL configurations of the infinite hole array. The sample without the DPL shows a dipole field pattern formed at the hole exit at the metal-silicon interface. The sample with the DPL shows the same dipole-like field pattern at the hole exit on the metal-silicon side, as well as a stronger field confinement above the hole entrance on the metal-air side.

Figure 3-10 shows the field distribution plot of the y-component of the magnetic field at the 0.58 THz resonance frequency. The simulated hole array with the DPL shows that at the metal-silicon interface, H_y is enhanced on the right and left sides of the hole exit, indicating stronger magnetic field coupling due to presence of the dielectric peg.

Figure 3-11 shows the simulated magnitude of the surface current $|I_s|$ on the metal film, both on the metal-air and metal-silicon sides, at 0.58 THz. The enhanced surface current due to the presence of the DPL both on the metal-air and metal-silicon indicates the strong influence of the magnetic field coupling on the overall transmission enhancement in the hole arrays featuring a DPL. The results of these simulations show enhanced coupling of the magnetic field through the

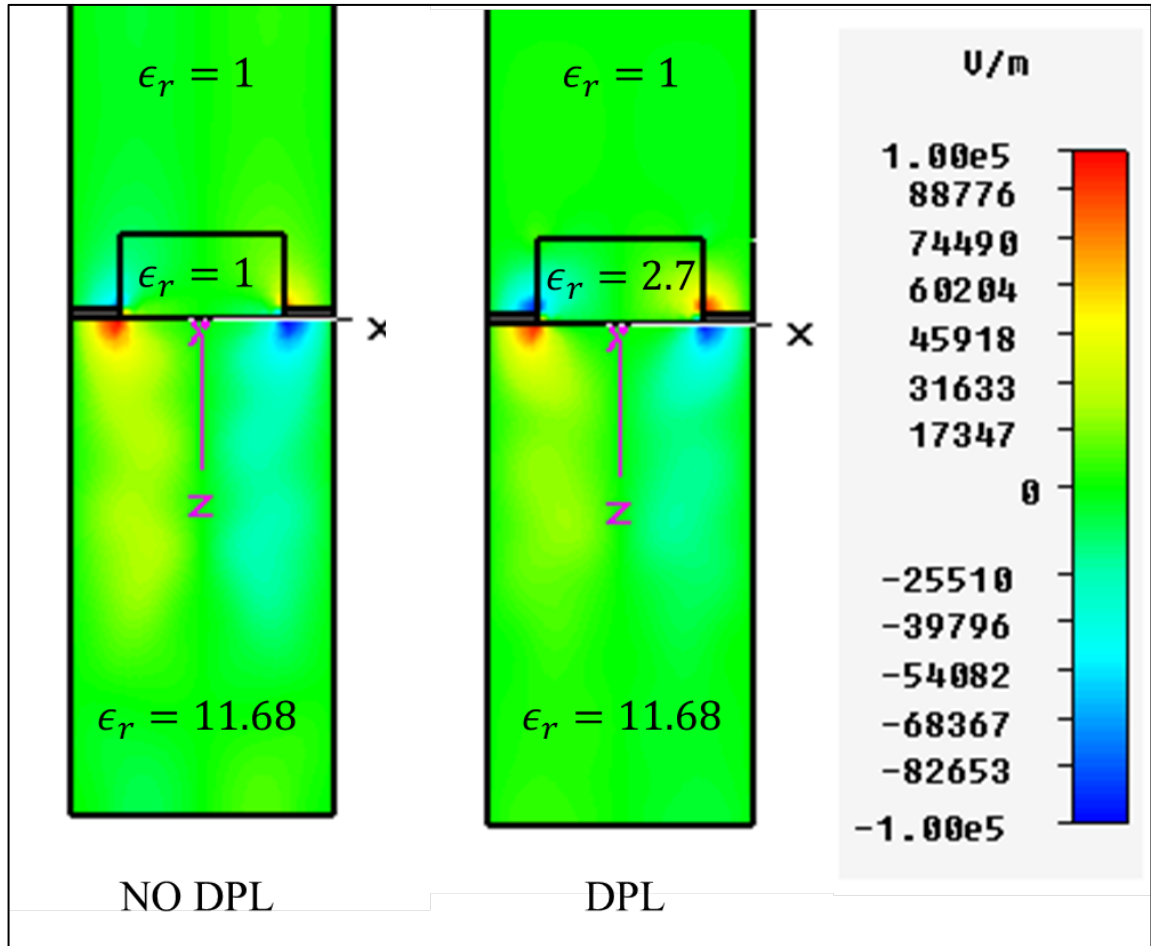


Figure 3-9 E_z field distribution at 0.58 THz with and without DPL. Slice is taken through center of a hole in yz plane.

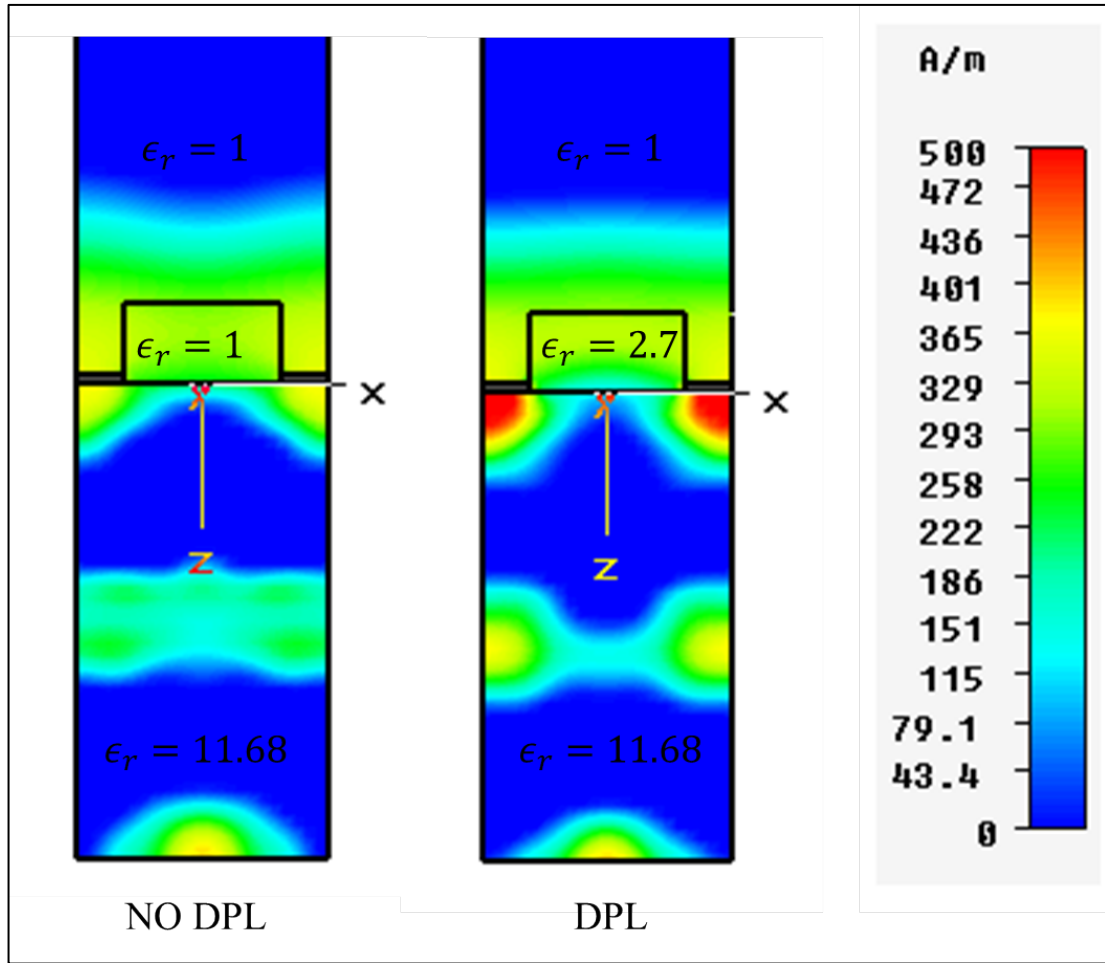


Figure 3-10 H_y field distribution at 0.58 THz with and without DPL. Slice is taken through center of a hole in yz plane.

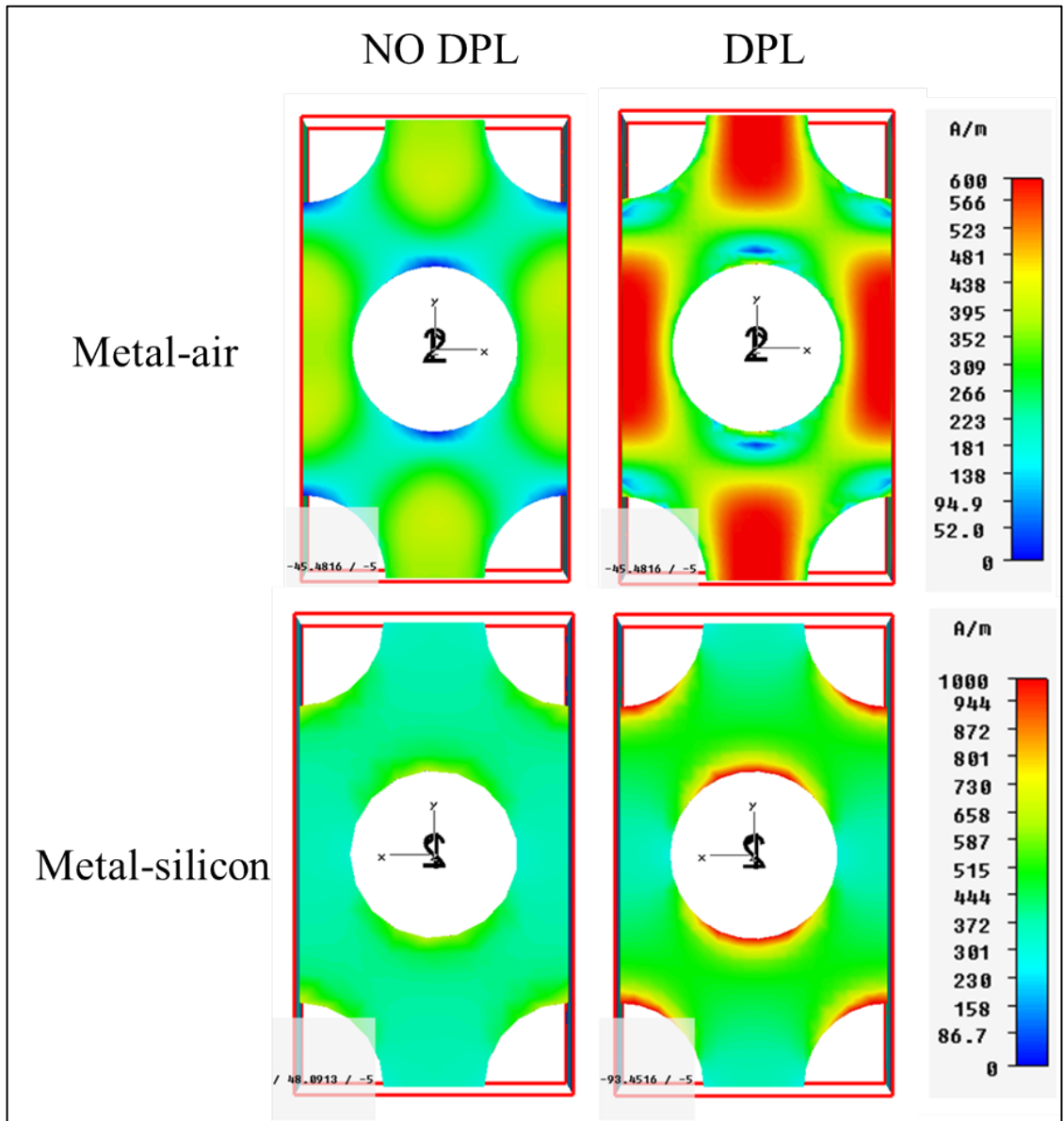


Figure 3-11 Surface current magnitude $|I_s|$ on metal film at 0.58 THz at metal-air and metal-silicon interfaces, with and without DPL.

holes, and as a result, enhanced surface current. The electric field distribution on the transmission (metal-silicon) side of the holes does not show as dramatic a difference with the addition of a DPL.

3.2.2 Higher Frequency Features

Unique spectral features are observed at the higher frequencies. Above $\epsilon_r = 1.25$, the spectra show sharp peaks between 1.5 THz and 2.4 THz. Clues to the mechanism underlying these peaks can be seen in the S11 (reflection) plots in [Figure 3-12](#). The S11 plots clearly show sharp features between 1.5 THz and 2.5 THz in the simulations with pegs containing dielectric constants greater than $\epsilon_r = 1.25$. At these higher dielectric constants, resonances inherent to the presence of the DPL lattice to appear. In general, these features tend to exhibit an overall red shift with increasing values of ϵ_r . One possible explanation of these features is that a hybrid plasmonic-photonic crystal effect occurs due to stop- and pass- bands formed by the periodic dielectric lattice. Indeed, without holes, the DPL in this study closely resembles the geometric organization of a photonic crystal array of dielectric rods [\[11, 91, 92\]](#) bounded on one side by a flat metal substrate. Though the behavior of dielectric rod array photonic crystals are well-characterized, the addition of the metal substrate is a non-trivial modification [\[93\]](#) which bears deeper study due to the complexities a SPP effect would bring about. This study seeks to point out this possible effect only as a qualitative means of explaining the higher frequency features. The $|I_s|$ distribution plots in [Figure 3-13](#) show that with addition of the DPL the $|I_s|$ field pattern is strikingly altered on the metal-silicon layer at 2.04 THz. The new modes introduced into the transmission spectra via the DPL clearly play a significant role in the transmission behavior at these higher frequencies.

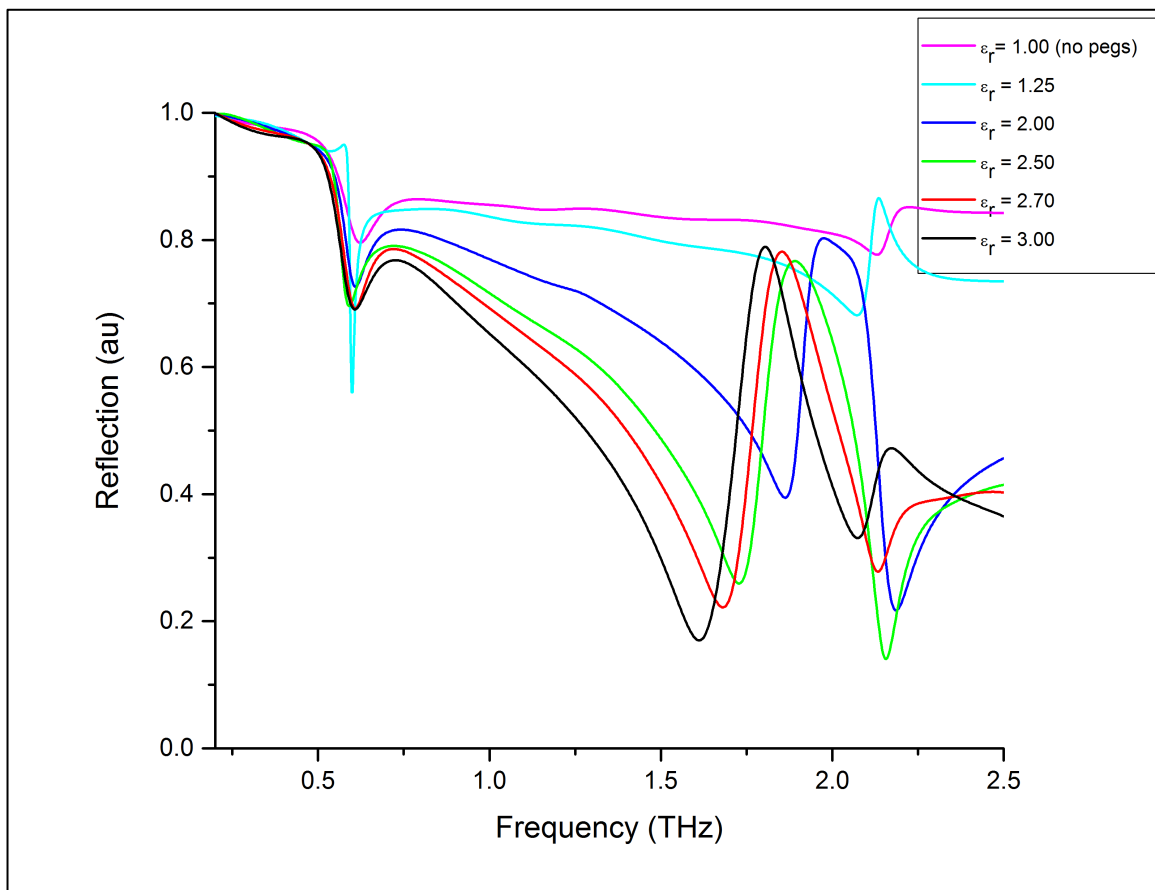


Figure 3-12 Simulated reflection spectra for infinite hole arrays with various dielectric constants of pegs in DPL.

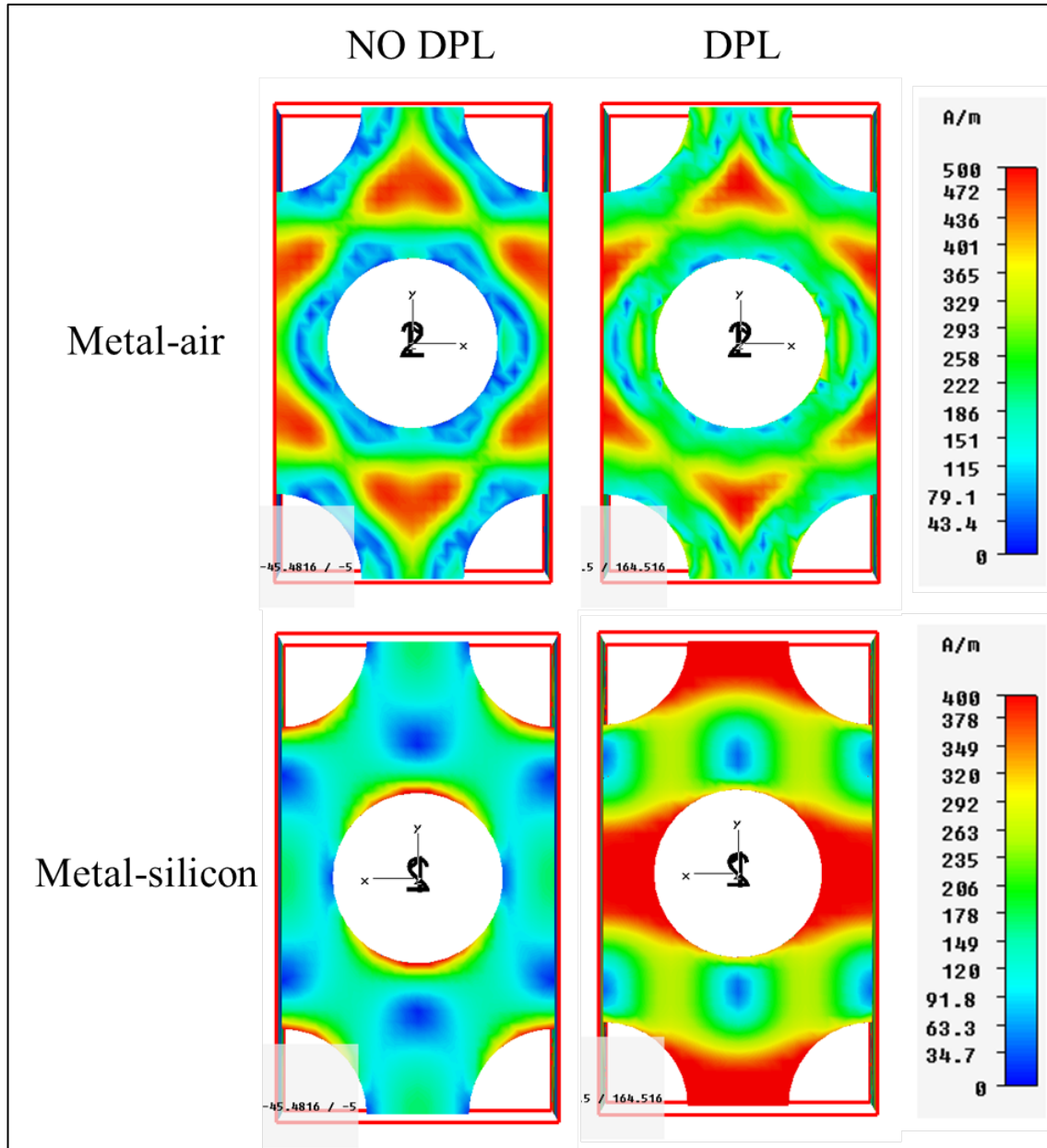


Figure 3-13 Surface current magnitude $|I_s|$ on metal film at 2.04 THz at metal-air and metal-silicon interfaces, with and without DPL.

CHAPTER IV

THZ-TDS EXPERIMENT

4.1 8F THz-TDS Beam System

For the experimental section of the study, a well-characterized 8F THz-TDS setup was used, as depicted in [Figure 4-1 \[19-21\]](#). This setup consisted of a femtosecond laser beam operating at 800 nm with 88 MHz repetition rate, optomechanically split into two paths: an excitation path and a probe path, each of 10 mW average power. The excitation beam was steered into a photoconductive stripline antenna ([Figure 4-1b](#)) and coupled into an air-tight measurement box via a silicon quasi-optic lens. The signal coupled from the silicon quasi-optic lens emerges as a coherent terahertz beam and gathered into paraboloidal mirror M1. The terahertz beam was then collimated by another paraboloidal mirror M2. A mounting post containing the fabricated heterostructure samples was positioned at the beam waist. The terahertz pulse emitted from the experimental structure enters two more paraboloidal mirrors M3 and M4 (optically symmetric to M3 and M4). In this instance, the purpose of the second two paraboloidal mirrors was to compress the beam and focus via a second silicon quasi-optic lens into a terahertz receiver chip.

A current amplifier with picoampere precision was located at the end of the receiver chip as schematically depicted in [Figure 4-1c](#). The probe beam was steered into the same terahertz receiver chip, where the probe beam and electrical signal generated by the excitation beams could

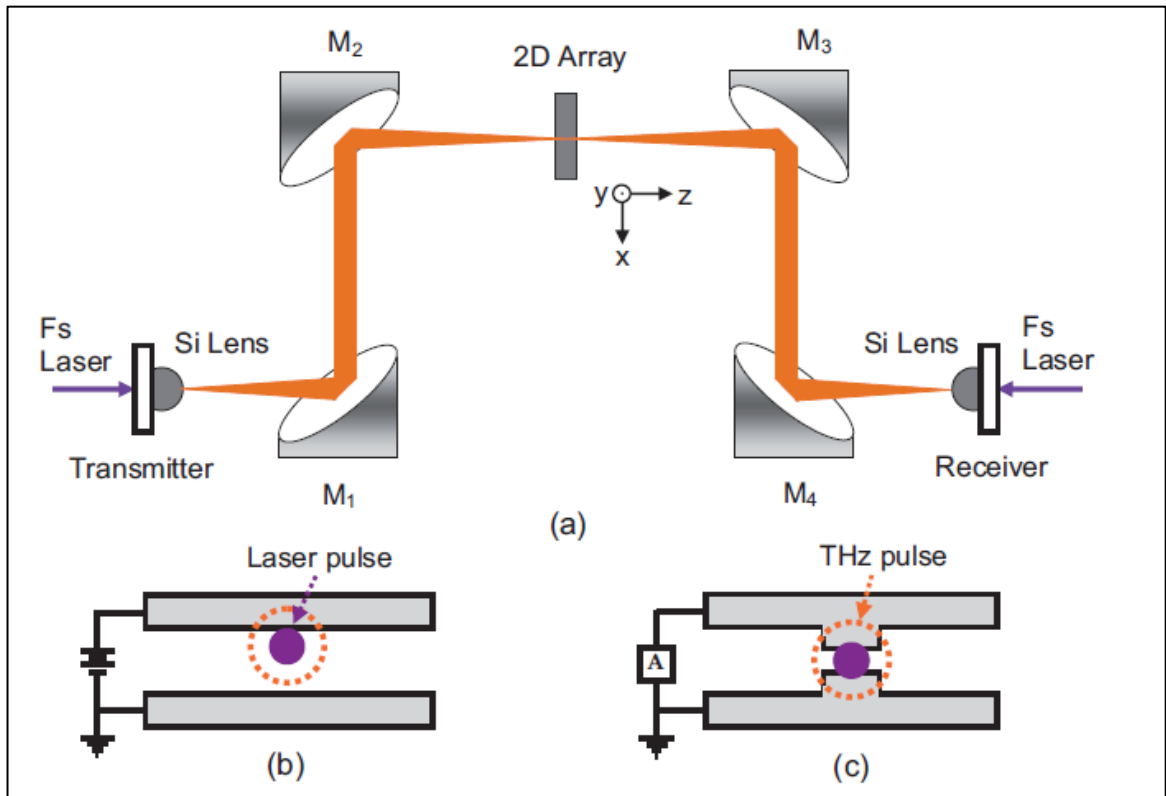


Figure 4-1 a) Schematic of the 8F THz-TDS system used to obtain the transmission spectra of the experimental heterostructures. M1 - M4 are paraboloidal mirrors. The fs excitation beam enters from the left of the schematic and the fs probe beam enters from the right. c) Schematic of transmitter chip for generation of terahertz beam. c) Schematic of receiver chip for detection of photoconductively switched electrical signals. From [19].

potentially intersect. If intersected, an electrical signal proportional to the excitation beam amplitude could be detected by the receiver and read out to computer via data acquisition (DAQ) system. The length of the beam path of the probe beam (and accordingly, the time instant of intersection with the excitation signal) was varied spatially via a motor-controlled translation stage. By syncing the known beam path of the probe beam with the amplitude output signal of the probe pulse autocorrelated with the transmitted pulse in the measurement box, a complete scan of the temporal response of the experimental heterostructures could be determined systematically via computer control. To obtain the frequency response of the samples, Fast Fourier Transform (FFT) of the output data was performed.

4.2 Fabrication of Plasmonic Heterostructures

Manufacturing the experimental samples followed the sequence of steps depicted in [Figure 4-2](#). A thin photoresist layer was spin-coated onto a 640 μm thick wafer of lightly doped p-type silicon. The silicon material had a resistivity of $20 \Omega \cdot \text{cm}$ and relative permittivity ϵ_r of 11.68 at the THz frequencies under investigation [\[47\]](#). Photolithographic exposure was performed using a mask of eleven experimental hole cluster patterns as shown in [Figure 3-5](#). After development and dissolution of the excess photoresist, a 350 nm thick aluminum layer was deposited on the surface of the remaining template. Next, the excess aluminum was lifted off, revealing the hole clusters.

The steps involved in DPL fabrication are summarized in [Figure 4-3](#). A 50 μm thick layer of Futurrex NR5-8000 negative photoresist material [\[94\]](#) was spin-coated on the surface of the bare metal hole cluster samples. The DPL mask was manually aligned to overlap the hole openings on the metal hole cluster layer. After photolithographic exposure, the array was developed and post-baked to harden the resulting dielectric pegs.

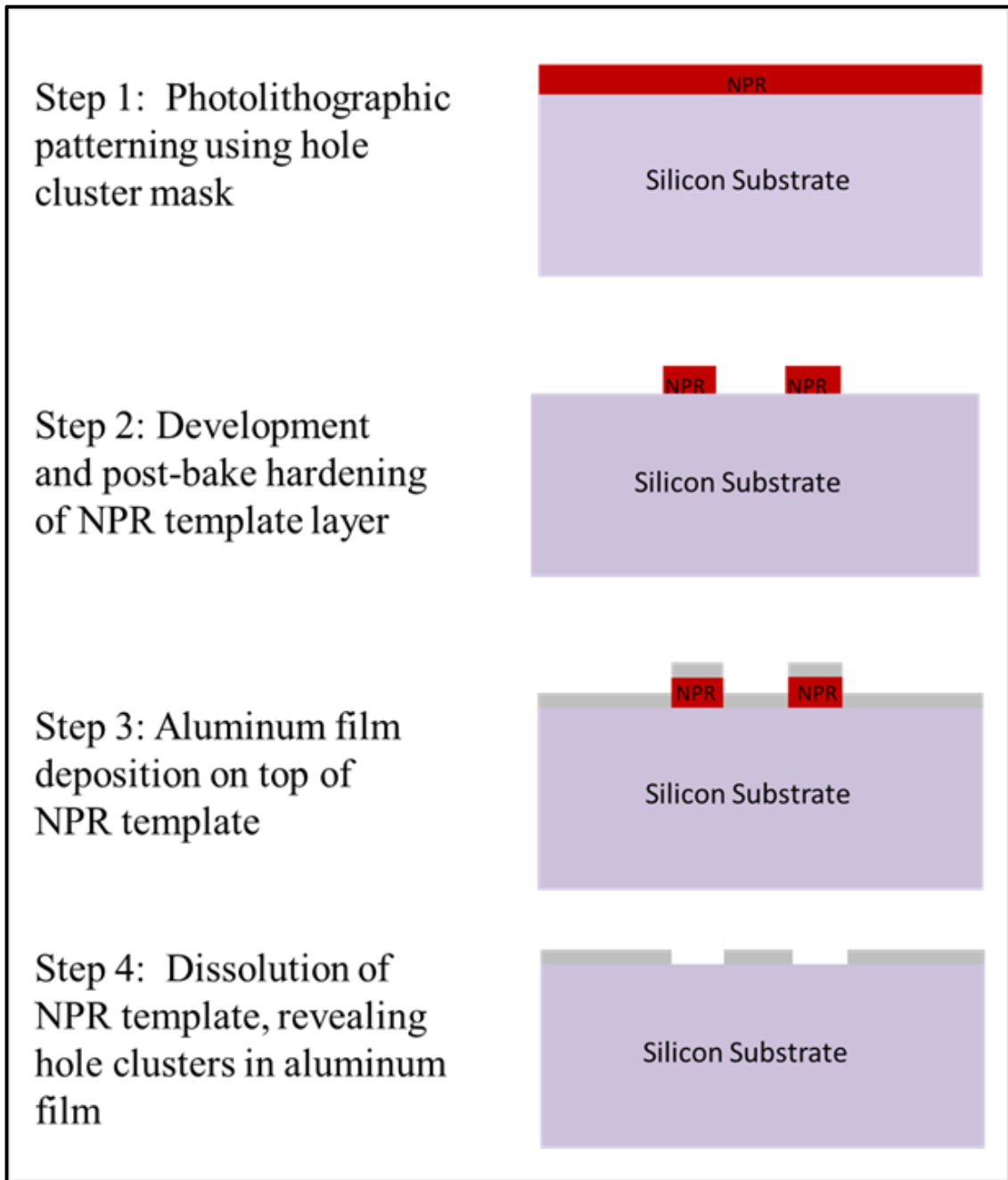


Figure 4-2 Fabrication steps for bare metal hole clusters (before addition of DPL).

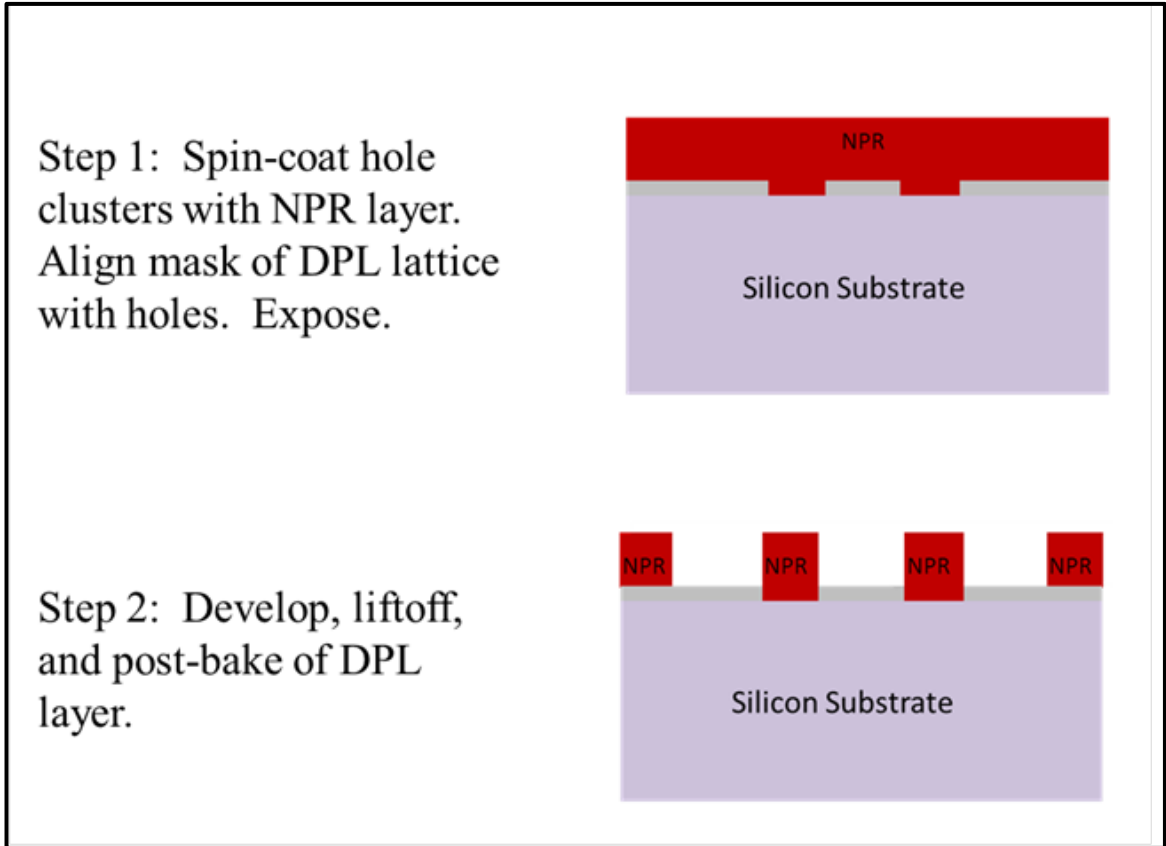


Figure 4-3 Fabrication steps for dielectric peg layer (DPL) on top of hole cluster samples.

After fabrication of the NPR pegs on top of the metal hole cluster samples was completed, the samples were immediately taken into the laboratory for measurement and data collection of their modified transmission spectra. Special care was taken to complete the measurements as soon as possible after fabrication so that the risk of material degradation of the NPR could be mitigated. Note: in future experiments using DPL structures meant to have a long shelf-life after fabrication, materials such as glass or quartz might be desirable substitutes [71-74].

4.3 Data Acquisition

Samples were aligned in the sample holder by adjusting their position in the xy-plane until maximum power output was obtained. This was an important step in that the samples were finite in size and radially symmetric, and as such the center of the hole clusters needed to be positioned as close to beam center as possible, to achieve repeatability and to ensure each sample received identical illumination within the 3.5 mm beam diameter. It should be noted that the terahertz beam used does not have a constant power distribution within its 3.5 mm beam diameter, so holes and features near the periphery of the experimental structure would receive less incident power than those located in the center. However, the widest samples measured in this study (h127 and r73) measured 2.02 mm in diameter. Assuming a Gaussian beam profile to represent the terahertz intensity distribution [95], the intensity at the edge of the largest samples can be estimated using the paraxial approximation for beam divergence [96]:

$$I(r, z) = I_0 \left(\frac{w_0}{w(z)} \right)^2 \exp \left(\frac{-2r^2}{w(z)^2} \right) , \quad (4-1)$$

where $I(r, z)$ is position-dependent beam intensity, I_0 is the intensity of the center of the beam at the waist, r is the radial distance from the beam axis, z is the position along the beam axis, w_0 is the beam waist, and $w(z)$ is the modified beam waist size along the beam axis as a function of

distance from w_0 . In this calculation, the sample is located directly at the waist, making $w(z) = w_0$. Assuming $w_0 = 1.75$ mm for a 3.5 mm diameter beam and $r = r_{h127} = 1.01$ mm for the maximum radial extent of the outer holes in sample h127, the beam intensity at the outer edge of the h127 sample drops to 51% of the intensity at the center of the sample. For the purposes of this study, this is assumed to be sufficiently bright enough illumination to compare each sample's transmission characteristics without having to consider the outer holes of the larger structures as insignificant in their contribution to the overall transmission. A qualitative illustration of the beam intensity distribution across the h127 sample is shown in [Figure 4-4](#).

The THz-TDS response of each sample was measured both with and without a DPL layer. A scan of a bare silicon wafer was measured as a reference before each scan of an experimental hole cluster structure was taken, in order to normalize off the frequency-dependent response of silicon from the transmission spectra of the hole cluster structures. All of the measurements for the samples without DPL were completed before fabricating the DPL layer on top of the bare metal hole clusters. The procedure for obtaining the THz-TDS response of the samples with the added DPL was identical to the procedure for the samples without the DPL. Data analysis was performed of the frequency-domain spectra, and the results are presented in the next chapter.

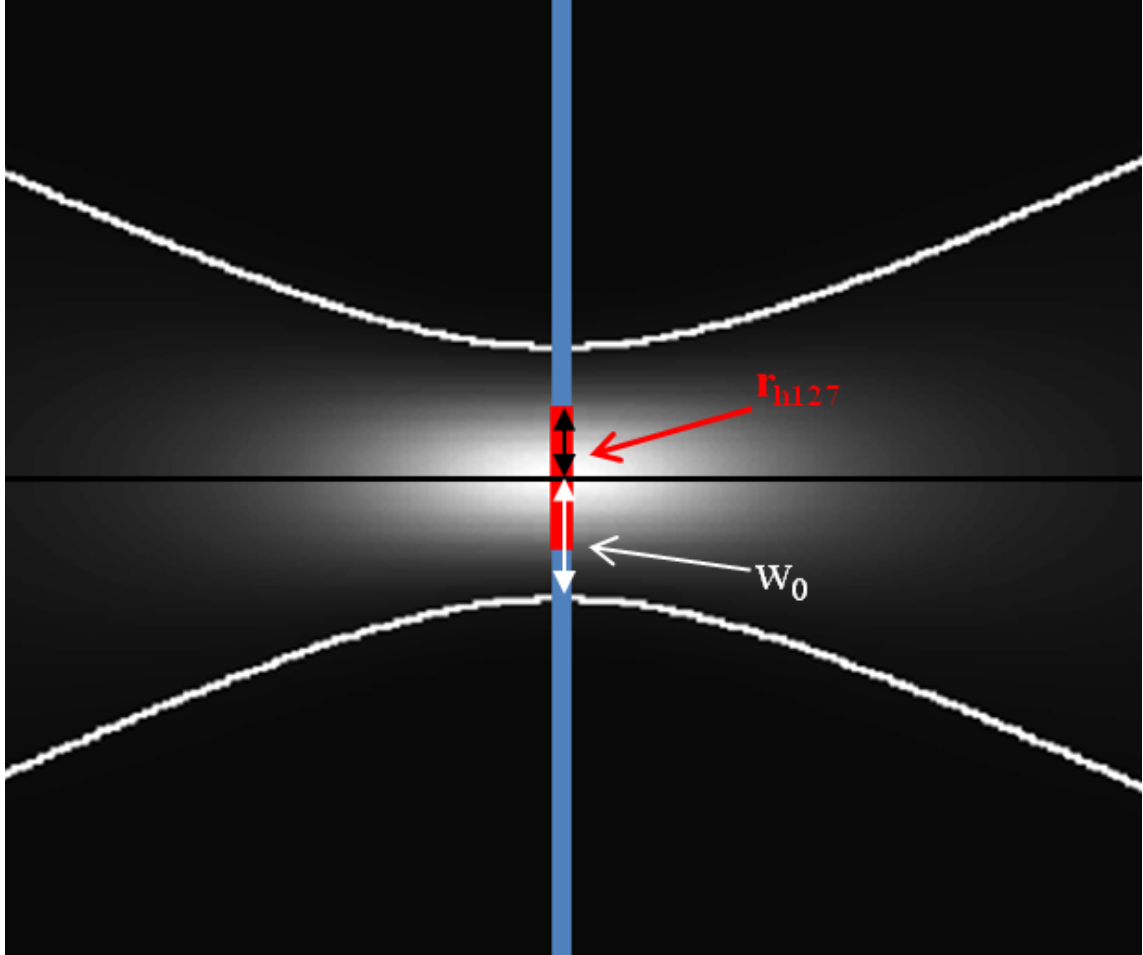


Figure 4-4 Conceptual illustration of beam divergence consideration in alignment of the larger samples measured in this study. The hyperbolic white lines illustrate the Gaussian beam divergence as it propagates through the beam waist. Position of h127 is shown within the intensity distribution of a typical Gaussian beam profile. The red area represents the spatial extent of region containing holes. In this diagram, the waist of the THz beam $w_0 = 1.75$ mm and $r_{h127} = 1.01$ mm. In this case, the intensity $I(r, z)$ of the beam at the edge of the h127 sample is 51% of the intensity I_0 at the center of the sample. Background image taken from [97].

CHAPTER V

RESULTS OF EXPERIMENT

This chapter presents the data obtained in the experimental portion of the study. Section 5.1 presents the transmission spectra obtained and compares the properties of the hole clusters with and without a DPL layer. The unique transmission characteristics specific to the main resonance in the “h” and “r” patterns of are dealt with in sections 5.1.1 and 5.1.2, respectively. Section 5.1.3 analyses the higher frequency features observed in some of the experimental samples. The transmission enhancement due to DPL seen in the two “rand” hole clusters is discussed in section 5.1.4. Section 5.2 presents a comparison of the experimental results for the finite-size hole clusters to the simulated results of infinitely periodic clusters. Section 5.2.1 compares the similarities and differences in the main resonance transmission enhancement. Section 5.2.2 compares the shape of main resonance peaks in the simulated and experimental data from the perspective of a Fano lineshape.

5.1 Transmission Spectra of Experimental Structures

A side by side comparison of the transmission spectra for the bare metal hole clusters is shown in [Figure 5-1](#). A distinct resonance peak in the normalized transmission is observed in samples h7, h19, r13, h37, r37, r73, h91, h127. A table with the measured peak characteristics is shown in

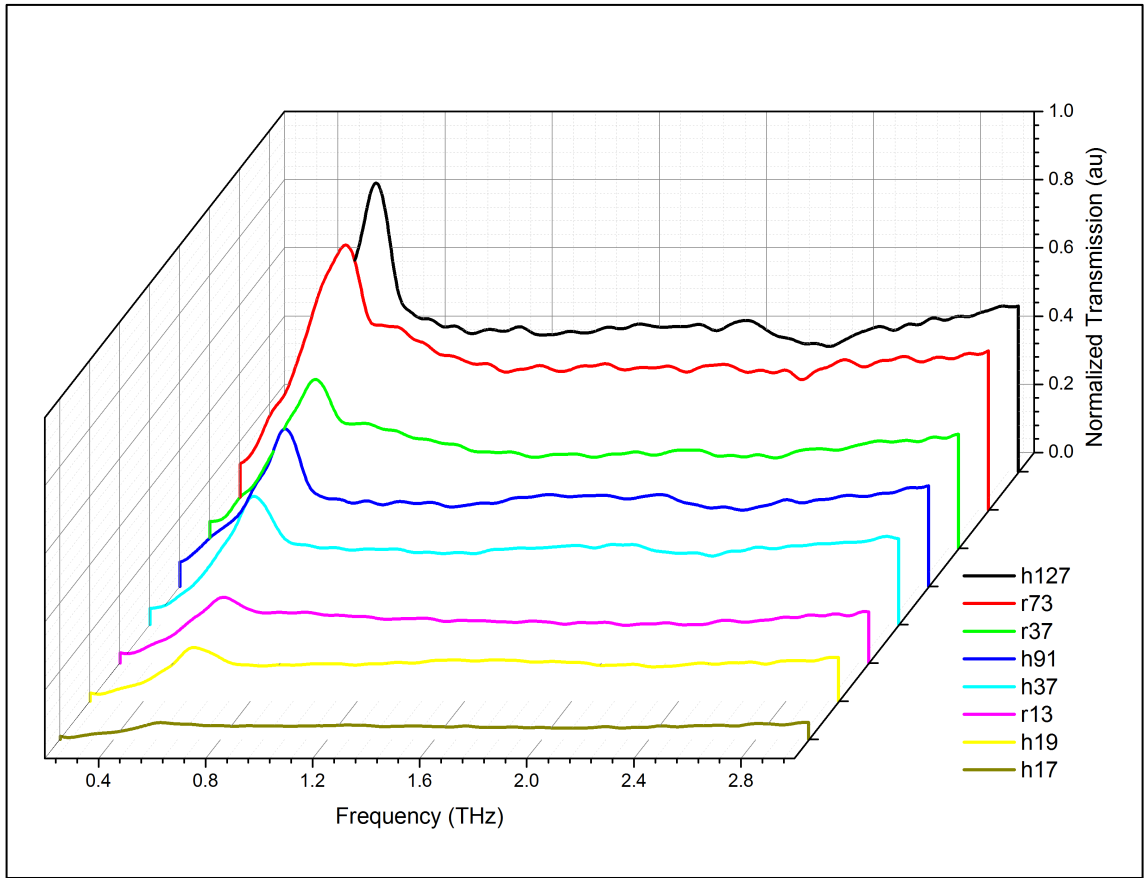


Figure 5-1 Comparison of Normalized Transmission spectra of metal hole arrays. Transmission spectra are normalized by porosity.

Cluster	Peak Height	Frequency (THz)	FWHM (THz)	Q Factor
h127	0.85	0.60	0.139	4.29
r73	0.78	0.60	0.190	3.13
r37	0.49	0.60	0.172	3.47
h91	0.46	0.59	0.124	4.77
h37	0.38	0.59	0.124	4.74
r13	0.19	0.59	0.110	5.33
h19	0.16	0.59	0.135	4.35
h7	0.05	0.58	0.146	3.95

Table 5-1 Peak data for metal hole clusters without dielectric peg layer (DPL)

[Table 5-1](#). The fundamental resonance peak in each sample was located between 0.58 and 0.60 THz. The normalized transmission peak height was not directly proportional to the number of holes in each sample. For instance, the r73 sample exhibited a peak transmission of 0.78 at 0.60 THz, where the p91 sample exhibited a peak transmission of 0.46 at 0.59THz.

A side by side comparison of the effect of the DPL on the normalized transmission of the hole clusters is shown below in [Figure 5-2](#). Each of the samples, except for h91, showed an increase in transmission at the fundamental resonance with addition of the DPL. [Table 5-2](#) shows the peak data obtained from the fundamental resonance of these spectra in tabular form.

The predicted peak resonance of the Al-Si interface is estimated by Eq. (1-5), using the terahertz approximation from Eq. (1-6). The value of k_R based on an infinite hexagonal lattice of holes of periodicity 160 μm comes from Eq. (2-5). For the lightly doped silicon used in this study, it is assumed that $\epsilon_d = 11.68$. The predicted SP resonance for the infinite hole array is located at 0.63THz.

5.1.1 Main Resonance Enhancement in “h” Clusters

[Figure 5-3](#) shows a comparison of the normalized transmission of the “h” clusters before and after addition of the DPL. For samples h19, h37, and h127 the height of the transmission peak is enhanced by 13%, 18%, and 17%, respectively, with addition of the DPL. The relation of hole number to transmission enhancement in “h” clusters can be visualized in [Figure 5-4](#). h91 shows a decrease in transmission with addition of DPL. This surprising result was confirmed in three separate THz-TDS scans and attributed to possible damage to some portion of the NPR layer,

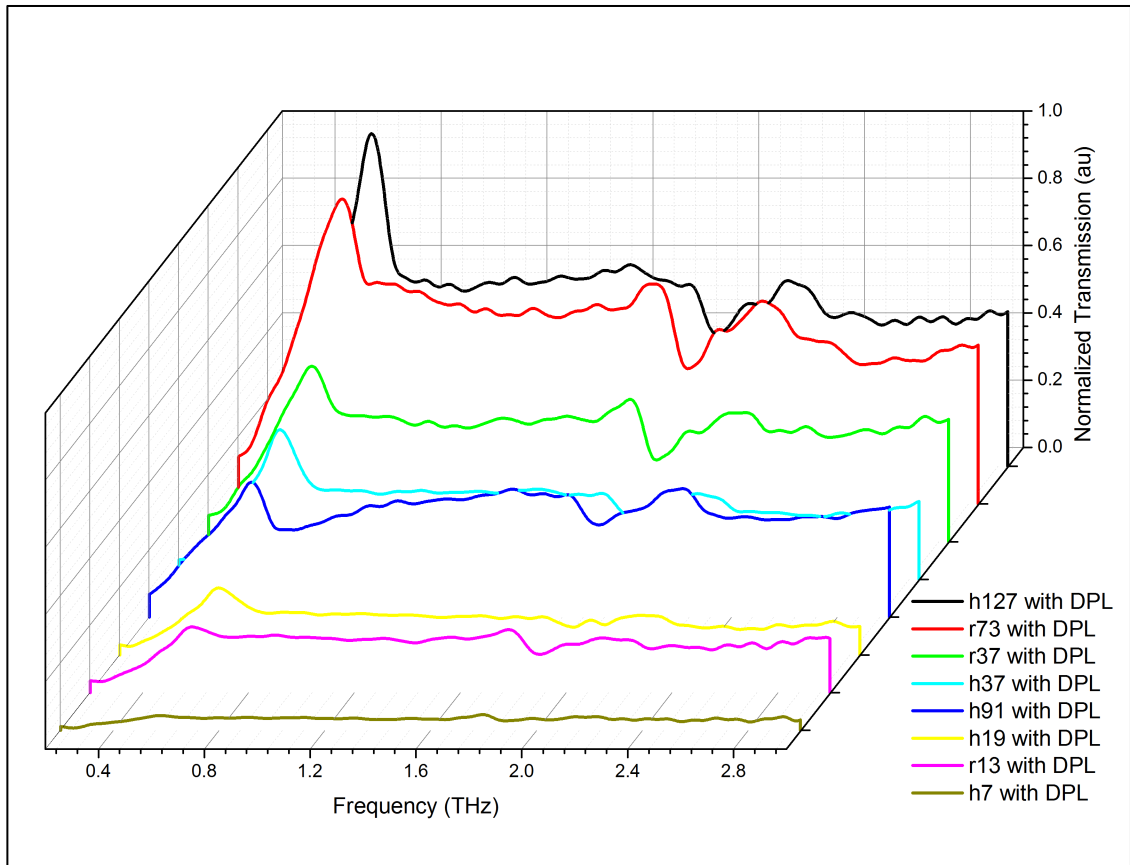


Figure 5-2 Comparison of Normalized Transmission spectra of metal hole arrays with added dielectric peg layer (DPL). Transmission spectra are normalized by porosity.

Cluster	Peak Height	Frequency (THz)	FWHM (THz)	Q Factor
h127	0.99	0.59	0.117	5.06
r73	0.91	0.59	0.154	3.86
r37	0.52	0.59	0.198	3.00
h37	0.45	0.58	0.124	4.68
h91	0.40	0.59	0.113	5.19
h19	0.20	0.57	0.128	4.49
r13	0.20	0.59	0.102	5.71
h7	0.04	0.58	0.088	6.58

Table 5-2 Peak data for metal hole clusters with dielectric peg layer (DPL)

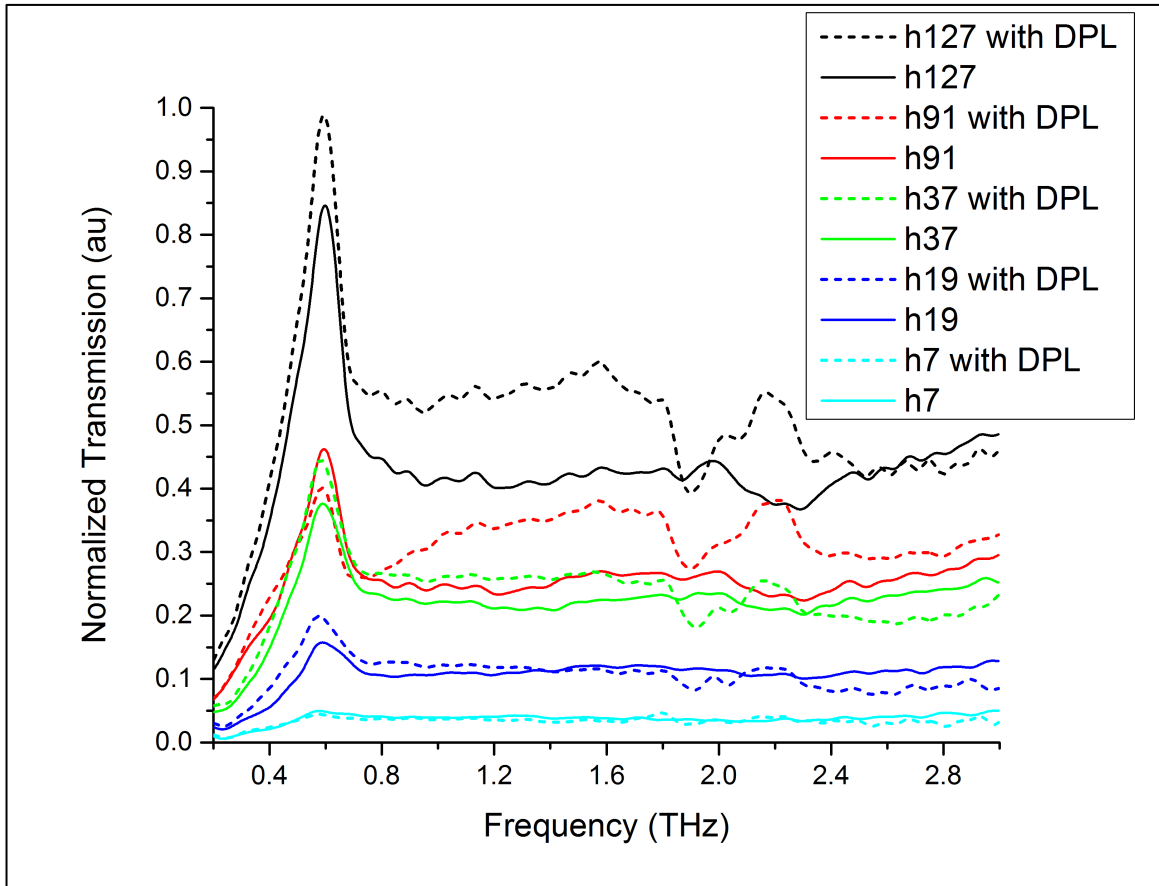


Figure 5-3 Normalized transmission spectra for "h" cluster samples with and without DPL (experimental).

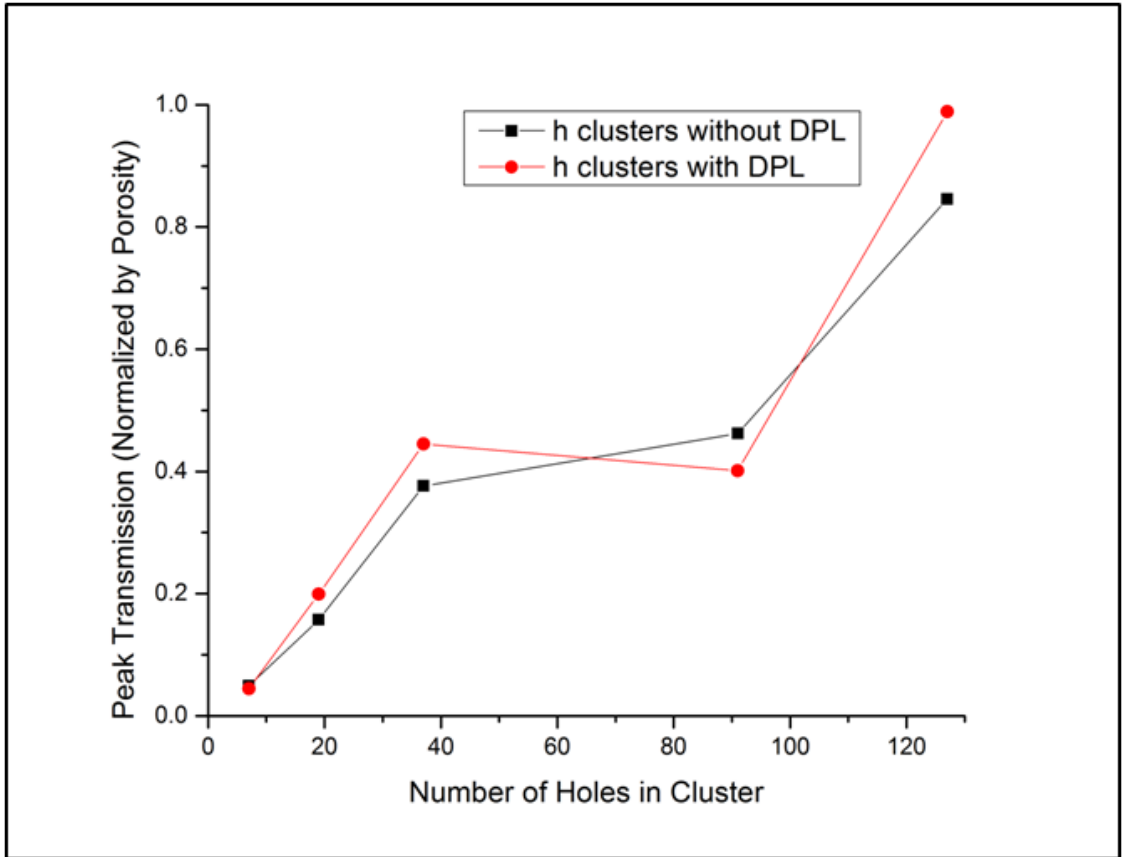


Figure 5-4 Effect of DPL on peak resonance height in "h" pattern hole clusters. Transmission values are normalized by porosity.

which is not specifically intended for open-air applications but rather for use in subtractive and mold steps during semiconductor fabrication processing [94]. A very weak signal was measured from the h7 cluster, containing only a slightly detectable “peak” at 0.58 THz. It is excluded from the DPL-vs.-non-DPL discussion here, because whether or not it classifies as a “peak” with meaningful properties for which to compare is subjective.

Assuming a Lorentzian peak fit, linewidth narrowing of 6%, 10%, and 19% is observed in samples h19, h91, and h127, respectively, with addition of DPL. The linewidth of h37 is not affected. It is likely that some error in these figures arises due to the degree of subjectivity involved in specification of the peak itself. In section 5.2.2, the peak shapes are reinvestigated using an asymmetric (Fano) peak fit, giving insight into other factors involved in the surface plasmon resonance behavior.

5.1.2 Main Resonance Enhancement in “r” Clusters

Figure 5-5 shows a comparison of the normalized transmission of the “r” clusters before and after addition of the DPL. The height of each sample’s main resonance peak was enhanced with addition of DPL. Samples r13, r37, and r73 showed transmission enhancements of 1.5%, 5.5%, and 17%, respectively. Figure 5-6 shows the relationship between number of holes in the r-clusters, peak transmission enhancement, and presence of a DPL.

Samples r37 and r73 each show a clearly defined peak centered around 0.59 THz with another small hump near 0.70 THz. This small hump is seen both with and without a DPL, and as such it is likely an artifact of the unique distribution of parallel \mathbf{k} vectors due to the empty rings in the

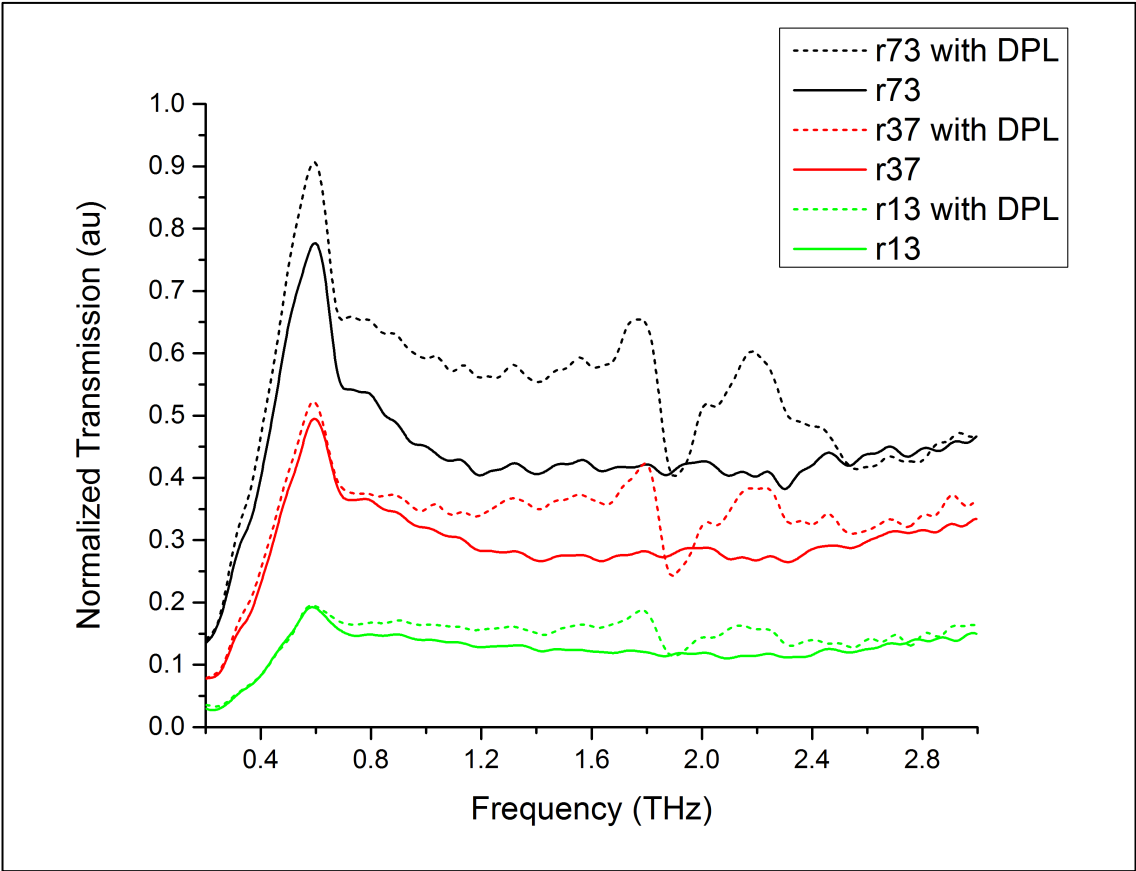


Figure 5-5 Normalized transmission spectra for "r" cluster samples with and without DPL (experimental).

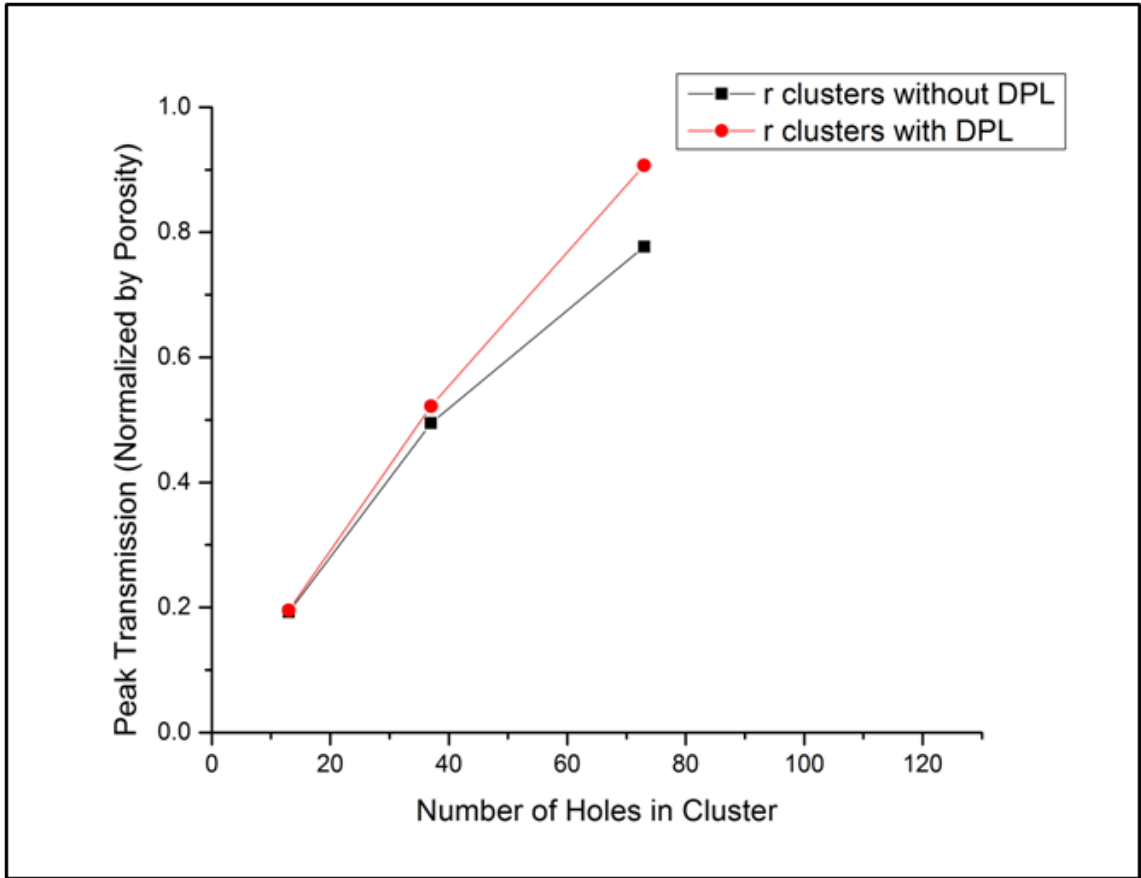


Figure 5-6 Effect of DPL on peak resonance height in "r" pattern hole clusters. Transmission values are normalized by porosity.

reciprocal lattice of the “r” clusters [1, 58]. This modified lattice likely accounts for this deviation from the well-defined resonance of a purely hexagonal lattice (or a large cluster of holes arranged in a hexagonal lattice such as an h127 cluster).

The peak fit parameter quantities reported in this section were based off a Lorentzian lineshape. It is evident on inspection however, that the peaks also exhibit some asymmetry. Section 5.1.4 looks at the asymmetrical nature of the 0.59 THz resonance.

5.1.3 Higher Frequency Features

Each sample exhibited to varying degree the presence of a collection of subtle mini-peaks between 1.75 and 2.5 THz with addition of DPL. These peaks were much more pronounced in the simulated spectra for infinite hole array systems. In Section 3.2.2 it was suggested that these are artifacts of the periodic peg lattice. This assumption is based on the fact that the dielectric constant of the peg material and, as a consequence, the effective dielectric constant at the surface of the sample causes clear frequency shifts in the higher frequency features in the simulation. Indeed, it is well known that periodic media create special conditions for electromagnetic waves which allow for the presence of resonances and band gaps [11, 88, 91, 92]. In the case of the experimental hole structures, however, the effect on transmission is much less dramatic. At minimum, it is worth mentioning that at some frequencies the behavior of the DPL lattice itself interferes with the transmission mechanism of the holes underneath it, but the effect appears well-isolated from the main resonance in the structures in this study.

5.1.4 Transmission Enhancement in “rand” Clusters

The hole array clusters featuring “rand” patterns (see [Figure 3-5](#)) exhibited transmission characteristics worthy of separate discussion from the ordered “h” and “r” clusters. The transmission plots are shown in [Figure 5-7](#). No normalization was performed on these spectra since no obvious periodicity exists in these patterns. Their measured spectra were strong enough to discern features, whereas in the single hole clusters no such features could be distinguished from noise.

For one, both with and without DPL the presence of the main resonance seen in the “h” and “r” clusters was much less pronounced. One interesting feature however was the strong amount of nonresonant transmission enhancement seen in the “rand” structures as seen with the DPL. Indeed, of all the structures tested in this study, the rand19 structure showed the most benefits in terms of enhanced energy transmission. Another distinct feature observed in the “rand” samples was the pronounced, albeit noisy, higher order features with addition of DPL in the 1.75-2.4THz range, much like the ones observed in the simulation and in some of the “h” and “r” clusters.

A possible source of the enhanced transmission of the “rand” clusters is that, though the coupling of SPs from hole to hole was limited in these structures due to absence of a highly periodic hole grating effect, the dielectric pegs helped assist the coupling of energy through the holes by means of the magnetic field more so than the electric field. As discussed in Section 3.2.1, the z-component of the electric field (related to SP strength at the metal surface) is not significantly altered at the metal-silicon interface with addition of the DPL, but the enhanced magnetic field between the holes at the metal-silicon interface indicates presence of a nonresonant coupling mechanism. If so, this would explain why both the amplitude of the peaks and the “featureless”

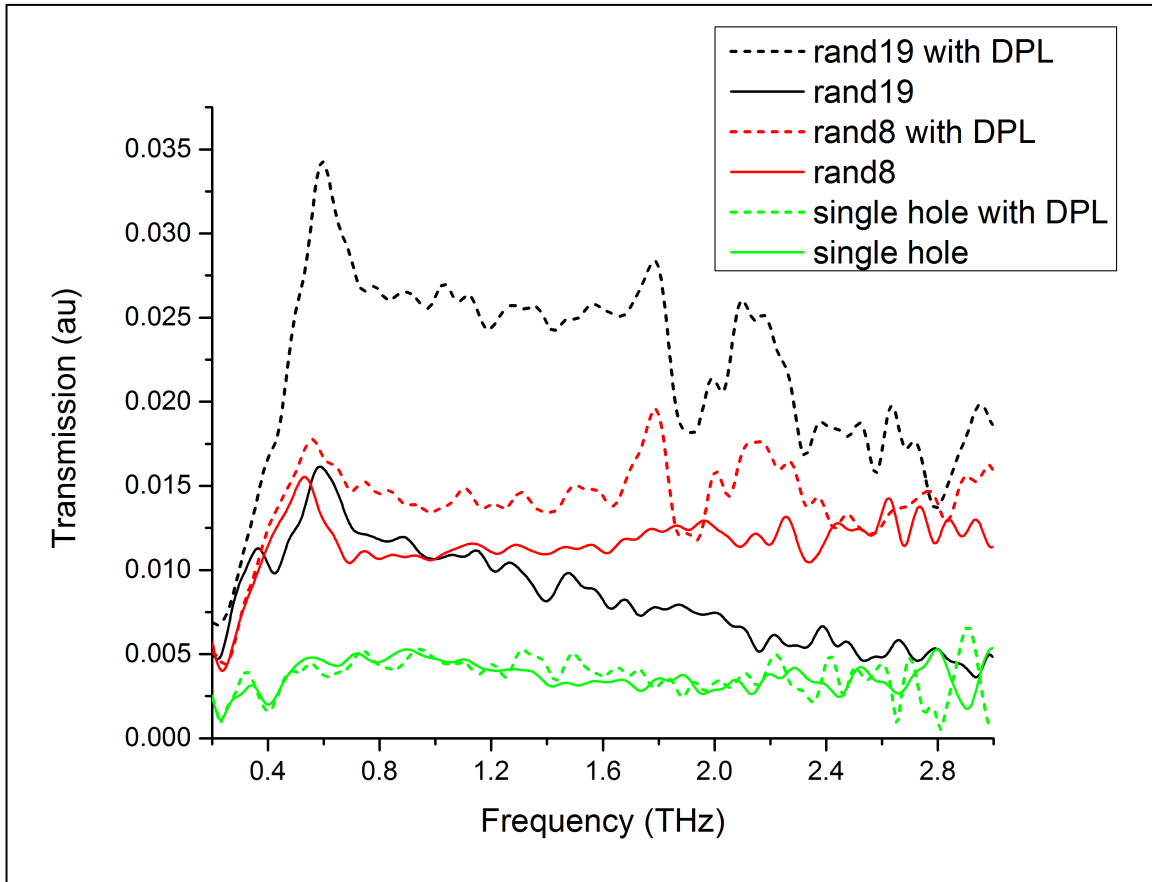


Figure 5-7 Measured transmission spectra for “aperiodic” cluster samples with and without DPL. Data is not normalized.

portions of the transmission spectrum for each hole cluster in this study was strengthened with addition of a DPL.

5.2 Comparison to Simulation

5.2.1 Enhancement of Main Resonance

The transmission properties of h127 and r73 are compared in [Figure 5-8](#) to the infinitely periodic hole array simulation presented in Chapter 3. It is apparent upon inspection that a similarity exists in the main resonance in all three structures. Generally speaking, the main resonance of each structure is centered in the frequency band 0.56-0.60 THz, and with addition of DPL the height of the main resonance is increased. This is in relatively good agreement with the theoretical prediction of the SP resonance at 0.63 THz. As was the case in Section 3.2.1 the discrepancy between the theoretical SP frequency and the experimentally observed resonance frequency is likely accounted for the fact that the 0.63 THz SP frequency does not take into account any nonresonant contributions. As will be discussed in 5.2.3, this is not merely a trivial point of distinction in this study.

5.2.2 Fano-like Characteristics of Main Resonance

A side by side peak fit experiment was performed on the DPL and non-DPL transmission characteristics of the infinite hole array simulation and experimental data from the h127 cluster. The main resonance peak was fit with a Fano lineshape between 0.2 and 0.7 THz. The spectra were normalized by assuming a peak value of unity for the non-DPL samples. Therefore any

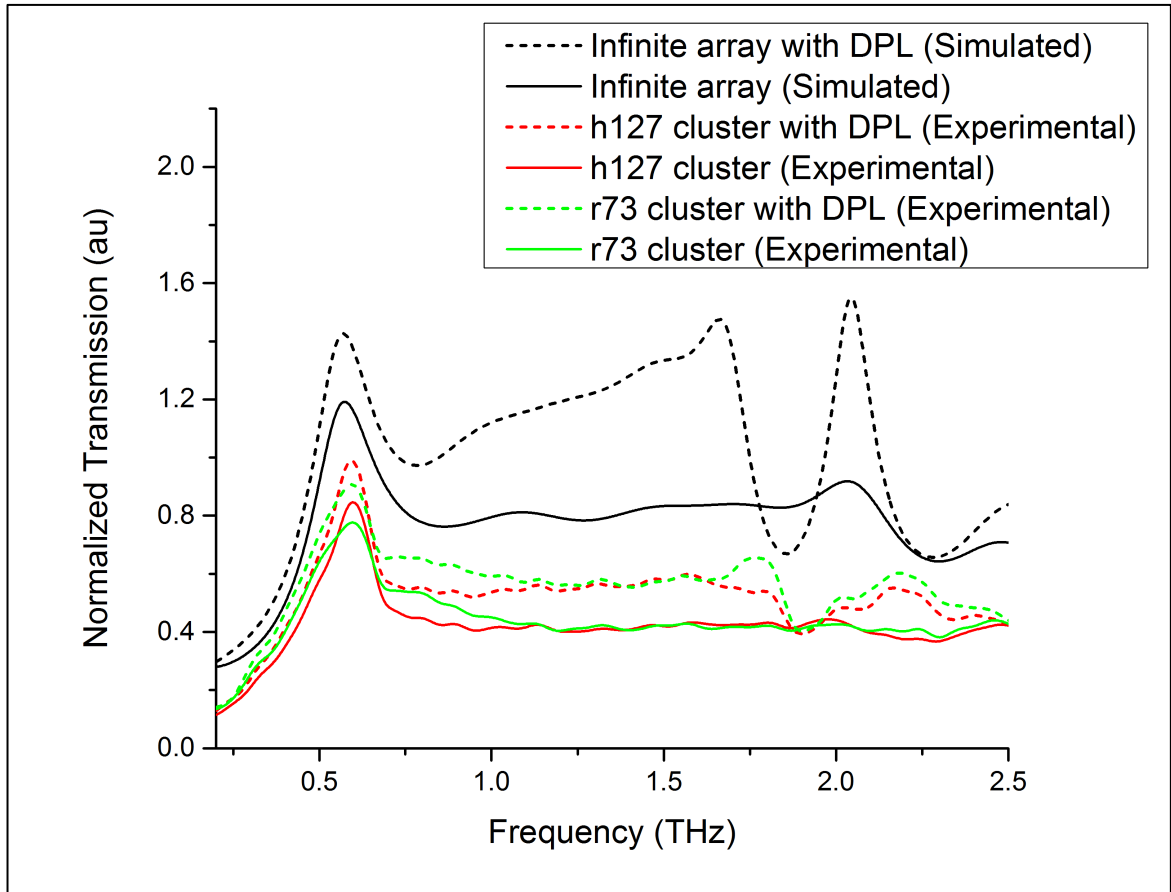


Figure 5-8 Comparison h127 and r73 clusters to simulation of infinitely periodic hole arrays (with and without DPL). Transmission is normalized by porosity.

transmission value above unity would indicate transmission enhancement due to DPL. This was done so that the lineshapes could be compared side by side for a hole cluster and for an infinitely periodic hole array, and also to compare the relative amplitude enhancement due to DPL for each structure. The plots shown in [Figure 5-9](#) indicate a stronger asymmetry in the hole cluster resonance than in the infinite hole array resonance. A look at the Fano parameters extracted from the fit confirms this ([Table 5.3](#)).

The closer to unity of the magnitude of asymmetry parameter q_v indicates a stronger Fano-like resonance, i.e. a stronger interaction with a discrete resonance with a slowly-varying background transmission [[21](#), [35](#), [50](#), [80](#), [85](#), [98](#), [99](#)]. It can be seen by comparing the magnitude of values of the asymmetry parameter q_v in [Table 5-3](#) that hole cluster samples show significantly stronger Fano-like asymmetry compared to the infinite hole array samples. Background transmission effects contributing to the asymmetry of the hole clusters could come from a number of places, but drawing a comparison between the cluster geometry of the hole clusters and a plasmonic oligomer could shed some light. That is, a finite-size hole cluster has a number of hole-to-hole scattering interactions that contribute to transmission, the most prominent of which being the $[\pm 1, 0]$ metal-silicon SP mode. On top of the SP behavior, scattering response of the cluster itself contributes to this transmission. In other words, there exists a contribution of modes inherent to both a) an infinite hole lattice perfectly discretized as an infinite combination of perfect unit cells and b) a scatterer the size and shape of an “h127” hole pattern, the latter of which being the “weaker” of the contributions near 0.59 THz. The potential to overlap these strong and weak resonances in plasmonic structures has already been explored in some detail [[35](#), [36](#), [82-86](#), [98](#), [99](#)], and in this study it is shown that direct access to engineering the dark component in a subwavelength hole cluster is possible *without adding extra holes or changing the hole cluster arrangement in any way*.

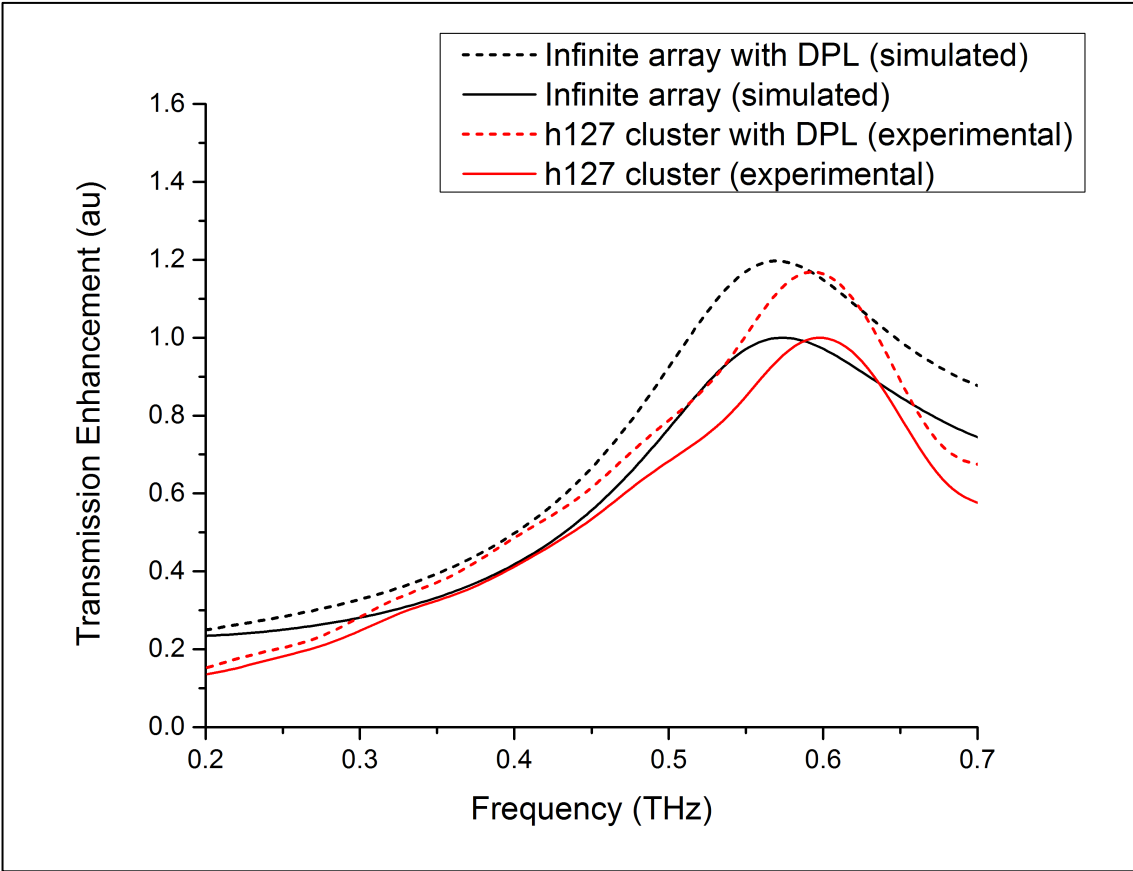


Figure 5-9 Side-by-side comparison of transmission enhancement of the main resonance peak shape due to DPL for a hole cluster (experimental) and infinite hole array (simulated). The hole array and hole cluster samples are normalized to the same peak value (unity) for non-DPL transmission, so that any transmission greater than unity is enhancement due to DPL layer.

	T_a	f_ν	T_b	$\Gamma_\nu/2\pi$	q_ν
h127	-0.18083	0.63572	1.07313	0.13967	-3.77502
h127 with DPL	-0.1364	0.62369	1.20638	0.13644	-4.65615
Infinite hole array	0.10312	0.58854	0.89913	0.14437	-1.87E18
Infinite hole array with DPL	0.10233	0.5853	1.09068	0.14518	-6.02E17

Table 5-3 Fano Parameters extracted from peaks in [Figure 5-9](#)

CHAPTER VI

CONCLUSION

This section summarizes the results of the experiment and simulation, and provides an interpretation of the results in the context of design of future nanophotonic device applications.

6.1 Summary of Results

This study has shown through simulation and experiment that cylindrical dielectric peg structures fabricated over the hole openings of a subwavelength scale aperture array enhances the transmission of terahertz radiation through the arrays. The expected normalized transmission enhancement is from 5% to nearly 20% depending on the arrangement and number of holes in the structure. It was shown that varying the pattern and spacing of finite-size arrays of holes affects the shape and height of the main surface plasmon resonance. Enhancement of the nonresonant component of the frequency spectrum is also observed. Analysis of the peak properties show that finite-size arrays show a Fano-like asymmetry. This Fano-like asymmetry is attributed to plasmonic hybridization, arising from a combination of molecular and atomic resonances similar to previous studies of finite-size plasmonic oligomers. Simulation indicates the dielectric layer in finite-size arrays in particular seems to enhance the coupling of magnetic field intensity as well as the induced surface current at the metal-dielectric interfaces. This enhanced nonresonant component can be described by the analogy of an effective widening of the holes due to the stronger field confinement near the hole openings.

6.2 Future Work

The structures studied in this experiment point towards new techniques of optimizing the design and fabrication of nanoscale photonic devices. If one of the key design specifications of such a device is to minimize size, maximize control of the system response shape, and maximize signal to noise, the hole-peg configuration presents an interesting option. In the vicinity of a single resonance such as the one near 0.58 THz seen in this study, one might be able to exert a good deal of control over the height and width of the resonance, without altering the resonant frequency, and without compromising transmitted signal strength, but rather boosting the signal. The boosting of the transmitted signal by fabrication of the DPL layer is a simple step in nanofabrication. The DPL itself in this study requires no special engineering, simply the overlay of an infinite, homogeneous periodic array of dielectric pegs on top of the hole openings. This simple step is enough that a small organization involved in manufacture of small nanophotonic sensors for instance, could have masks in storage that, when they needed them, they could overlay on top of a given sample to improve its performance. Also, this overlay step could improve the research and development of structures without DPL in the area of testing. That is, the DPL could be added in the investigation of the robustness of a specific design under certain conditions, for instance, to see if added corrugation arising from whatever reason (imperfections in fabrication process, juxtaposition next to a similar nanostructured object, decay of surface properties) has an undesirably large influence on the resonance of the system. Unlike systems of overlayers using metallic nanoparticles [23, 75-78], dielectric nanoparticles do not exhibit in and of themselves a localized plasmonic mode, further helping to enhance the main resonance but isolate it from corruption by other spectrally adjacent plasmonic effects.

As photonic devices become smaller and smaller, new opportunities in the history of technology become wide open. The closer the scientific community comes to engineering every facet of an

effect, the closer humanity comes to optimizing its energy consumption on a large scale, and optimizing the decision processes involved in improving the devices of the future. Analogies from older fields of study gain new momentum in light of new technologies that begin to develop new modes of engineering design. As mankind starts replacing some of the more outdated electronic technologies with light technology, anything is possible. It is the goal of this thesis to present one of the possibilities towards the end goal of exploring the frontiers of plasmonic device engineering, and to pose a potentially helpful perspective of looking at some aspects of the rapidly growing field of surface plasmon resonances.

REFERENCES

- [1] J. A. Stratton, *Electromagnetic Theory*. New York: McGraw-Hill, 1941.
- [2] H. A. Bethe, "Theory of Diffraction by Small Holes," *The Physical Review*, pp. 66 (7 and 8), 163-182, 1944.
- [3] A. Roberts, "Electromagnetic Theory of Diffraction by a Circular Aperture in a Thick, Perfectly Conducting Screen," *Journal of the Optical Society of America a-Optics Image Science and Vision*, vol. 4, pp. 1970-1983, Oct 1987.
- [4] F. de León-Pérez, G. Brucoli, F. J. García-Vidal, and L. Martín-Moreno, "Theory on the scattering of light and surface plasmon polaritons by arrays of holes and dimples in a metal film," *New Journal of Physics*, vol. 10, p. 105017, 2008.
- [5] Z. C. Ruan and M. Qiu, "Enhanced transmission through periodic arrays of subwavelength holes: The role of localized waveguide resonances," *Physical Review Letters*, vol. 96, Jun 16 2006.
- [6] M. A. Ordal, R. J. Bell, R. W. Alexander, Jr., L. L. Long, and M. R. Querry, "Optical properties of fourteen metals in the infrared and far infrared: Al, Co, Cu, Au, Fe, Pb, Mo, Ni, Pd, Pt, Ag, Ti, V, and W," *Appl Opt*, vol. 24, p. 4493, Dec 15 1985.
- [7] H. Raether, *Surface Plasmons on Smooth and Rough Surfaces and on Gratings*. New York: Springer-Verlag, 1988.
- [8] M. Ohtsu and K. Kobayashi, *Optical Near Fields: Introduction to Classical and Quantum Theories of Electromagnetic Phenomena at the Nanoscale*. New York: Springer, 2004.

- [9] J. Tominaga, *Optical Nanotechnologies: The Manipulation of Surface and Local Plasmons*. New York: Springer, 2003.
- [10] D. W. Pohl, "Near-Field Optics and the Surface Plasmon Polariton," in *Near-Field Optics and Surface Plasmon Polaritons*, ed New York: Springer-Verlag Berlin Heidelberg, 2001, pp. 1-13.
- [11] L. Novotny and B. Hecht, *Principles of Nano-Optics*. Cambridge, UK: Cambridge University Press, 2006.
- [12] T. W. Ebbesen, H. J. Lezec, H. F. Ghaemi, T. Thio, and P. A. Wolff, "Extraordinary optical transmission through sub-wavelength hole arrays," *Nature*, vol. 391, pp. 667-669, Feb 12 1998.
- [13] H. J. Lezec and T. Thio, "Diffracted evanescent wave model for enhanced and suppressed optical transmission through subwavelength hole arrays," *Optics Express*, vol. 12, pp. 3629-3651, 2004.
- [14] L. Zhang, C. Y. Chan, J. Li, and H. C. Ong, "Rational design of high performance surface plasmon resonance sensors based on two-dimensional metallic hole arrays," *Opt Express*, vol. 20, pp. 12610-21, May 21 2012.
- [15] R. Gordon, A. G. Brolo, D. Sinton, and K. L. Kavanagh, "Resonant optical transmission through hole-arrays in metal films: physics and applications," *Laser & Photonics Reviews*, vol. 4, pp. 311-335, 2009.
- [16] F. J. Garcia-Vidal, L. Martin-Moreno, T. W. Ebbesen, and L. Kuipers, "Light passing through subwavelength apertures," *Reviews of Modern Physics*, vol. 82, pp. 729-787, Jan-Mar 2010.
- [17] A. E. Miroshnichenko, S. Flach, and Y. S. Kivshar, "Fano resonances in nanoscale structures," *Reviews of Modern Physics*, vol. 82, pp. 2257-2298, Aug 11 2010.
- [18] N. J. Halas, S. Lal, W. S. Chang, S. Link, and P. Nordlander, "Plasmons in strongly coupled metallic nanostructures," *Chem Rev*, vol. 111, pp. 3913-61, Jun 8 2011.

- [19] W. Zhang, "Resonant terahertz transmission in plasmonic arrays of subwavelength holes," *European Physical Journal-Applied Physics*, vol. 43, pp. 1-18, Jul 2008.
- [20] A. K. Azad, "Resonant Terahertz Transmission of Plasmonic Subwavelength Hole Arrays," Doctoral Dissertation, Electrical Engineering, Oklahoma State University, Stillwater, OK, 2006.
- [21] X. Lu, "Studies of Surface Plasmons and Localized Surface Plasmons at Terahertz Frequencies," Doctoral Dissertation, Electrical Engineering, Oklahoma State University, Stillwater, OK, 2009.
- [22] C. Genet and T. W. Ebbesen, "Light in tiny holes," *Nature*, vol. 445, pp. 39-46, Jan 4 2007.
- [23] S.-m. Kim, W. Zhang, and B. T. Cunningham, "Photonic crystals with SiO₂-Ag "post-cap" nanostructure coatings for surface enhanced Raman spectroscopy," *Applied Physics Letters*, vol. 93, p. 143112, 2008.
- [24] A. J. Pasquale, B. M. Reinhard, and L. Dal Negro, "Engineering photonic-plasmonic coupling in metal nanoparticle necklaces," *ACS Nano*, vol. 5, pp. 6578-85, Aug 23 2011.
- [25] W. L. Barnes, A. Dereux, and T. W. Ebbesen, "Surface plasmon subwavelength optics," *Nature*, vol. 424, pp. 824-30, Aug 14 2003.
- [26] A. J. Baragwanath, M. C. Rosamond, A. J. Gallant, and J. M. Chamberlain, "Time-of-Flight Model for the Extraordinary Transmission Through Periodic Arrays of Subwavelength Apertures at THz Frequencies," *Plasmonics*, vol. 6, pp. 625-636, Dec 2011.
- [27] B. K. Juluri, S. C. Lin, T. R. Walker, L. Jensen, and T. J. Huang, "Propagation of designer surface plasmons in structured conductor surfaces with parabolic gradient index," *Opt Express*, vol. 17, pp. 2997-3006, Feb 16 2009.

- [28] J. Zhang and G. P. Wang, "Simultaneous realization of transmission enhancement and directional beaming of dual-wavelength light by a metal nanoslit," *Opt Express*, vol. 17, pp. 9543-8, Jun 8 2009.
- [29] A. Agrawal, Z. V. Vardeny, and A. Nahata, "Engineering the dielectric function of plasmonic lattices," *Opt Express*, vol. 16, pp. 9601-13, Jun 23 2008.
- [30] S. Wang, D. F. Pile, C. Sun, and X. Zhang, "Nanopin plasmonic resonator array and its optical properties," *Nano Lett*, vol. 7, pp. 1076-80, Apr 2007.
- [31] Z. B. Li, Y. H. Yang, X. T. Kong, W. Y. Zhou, and J. G. Tian, "Enhanced transmission through a subwavelength slit surrounded by periodic dielectric bars above the metal surface," *Journal of Optics a-Pure and Applied Optics*, vol. 10, p. 095202, Sep 2008.
- [32] J. B. Pendry and S. A. Ramakrishna, "Near-field lenses in two dimensions," *Journal of Physics-Condensed Matter*, vol. 14, pp. 8463-8479, Sep 15 2002.
- [33] N. F. Yu, Q. J. Wang, C. Pflugl, L. Diehl, F. Capasso, T. Edamura, *et al.*, "Semiconductor lasers with integrated plasmonic polarizers," *Applied Physics Letters*, vol. 94, p. 151101, Apr 13 2009.
- [34] N. F. Yu, R. Blanchard, J. Fan, F. Capasso, T. Edamura, M. Yamanishi, *et al.*, "Small divergence edge-emitting semiconductor lasers with two-dimensional plasmonic collimators," *Applied Physics Letters*, vol. 93, p. 181101, Nov 3 2008.
- [35] B. Luk'yanchuk, N. I. Zheludev, S. A. Maier, N. J. Halas, P. Nordlander, H. Giessen, *et al.*, "The Fano resonance in plasmonic nanostructures and metamaterials," *Nat Mater*, vol. 9, pp. 707-15, Sep 2010.
- [36] W. S. Chang, J. B. Lassiter, P. Swanglap, H. Sobhani, S. Khatua, P. Nordlander, *et al.*, "A plasmonic Fano switch," *Nano Lett*, vol. 12, pp. 4977-82, Sep 12 2012.
- [37] F. Hao, P. Nordlander, M. T. Burnett, and S. A. Maier, "Enhanced tunability and linewidth sharpening of plasmon resonances in hybridized metallic ring/disk nanocavities," *Physical Review B*, vol. 76, p. 245417, Dec 2007.

- [38] E. Cubukcu, N. F. Yu, E. J. Smythe, L. Diehl, K. B. Crozier, and F. Capasso, "Plasmonic Laser Antennas and Related Devices," *Ieee Journal of Selected Topics in Quantum Electronics*, vol. 14, pp. 1448-1461, Nov-Dec 2008.
- [39] E. Altewischer, M. P. van Exter, and J. P. Woerdman, "Plasmon-assisted transmission of entangled photons," *Nature*, vol. 418, pp. 304-6, Jul 18 2002.
- [40] J. B. Pendry, L. Martin-Moreno, and F. J. Garcia-Vidal, "Mimicking surface plasmons with structured surfaces," *Science*, vol. 305, pp. 847-8, Aug 6 2004.
- [41] F. J. Garcia-Vidal, L. Martin-Moreno, and J. B. Pendry, "Surfaces with holes in them: new plasmonic metamaterials," *Journal of Optics a-Pure and Applied Optics*, vol. 7, pp. S97-S101, Feb 2005.
- [42] H. Raether, "Surface plasma oscillations and their applications," in *Physics of Thin Films*. vol. 9, G. Hass, M. H. Francombe, and R. W. Hoffman, Eds., ed New York: Academic Press, 1977, p. 316.
- [43] J. Zhang, L. Zhang, and W. Xu, "Surface plasmon polaritons: physics and applications," *Journal of Physics D: Applied Physics*, vol. 45, p. 113001, 2012.
- [44] F. Przybilla, A. Degiron, C. Genet, T. W. Ebbesen, F. de Leon-Perez, J. Bravo-Abad, *et al.*, "Efficiency and finite size effects in enhanced transmission through subwavelength apertures," *Optics Express*, vol. 16, pp. 9571-9579, Jun 23 2008.
- [45] A. Agrawal, H. Cao, and A. Nahata, "Time-domain analysis of enhanced transmission through a single subwavelength aperture," *Optics Express*, vol. 13, pp. 3535-3542, May 2 2005.
- [46] A. Agrawal, T. Matsui, Z. V. Vardeny, and A. Nahata, "Terahertz transmission properties of quasiperiodic and aperiodic aperture arrays," *Journal of the Optical Society of America B-Optical Physics*, vol. 24, pp. 2545-2555, Sep 2007.
- [47] A. K. Azad and W. Zhang, "Resonant terahertz transmission in subwavelength metallic hole arrays of sub-skin-depth thickness," *Opt Lett*, vol. 30, pp. 2945-7, Nov 1 2005.

- [48] A. K. Azad, Y. Zhao, and W. Zhang, "Transmission properties of terahertz pulses through an ultrathin subwavelength silicon hole array," *Applied Physics Letters*, vol. 86, p. 141102, Apr 4 2005.
- [49] A. K. Azad, Y. Zhao, W. Zhang, and M. He, "Effect of dielectric properties of metals on terahertz transmission subwavelength hole arrays," *Opt Lett*, vol. 31, pp. 2637-9, Sep 1 2006.
- [50] J. G. Han, A. K. Azad, M. F. Gong, X. C. Lu, and W. L. Zhang, "Coupling between surface plasmons and nonresonant transmission in subwavelength holes at terahertz frequencies," *Applied Physics Letters*, vol. 91, p. 071122, Aug 13 2007.
- [51] J. B. Masson, A. Podzorov, and G. Gallot, "Extended Fano model of Extraordinary Electromagnetic Transmission through subwavelength hole arrays in the terahertz domain," *Optics Express*, vol. 17, pp. 15280-15291, Aug 17 2009.
- [52] F. Miyamaru and M. Hangyo, "Finite size effect of transmission property for metal hole arrays in subterahertz region," *Applied Physics Letters*, vol. 84, pp. 2742-2744, Apr 12 2004.
- [53] D. Qu, D. Grischkowsky, and W. Zhang, "Terahertz transmission properties of thin, subwavelength metallic hole arrays," *Opt Lett*, vol. 29, pp. 896-8, Apr 15 2004.
- [54] G. Goubau, "Surface Waves and Their Application to Transmission Lines," *Journal of Applied Physics*, vol. 21, pp. 1119-1128, 1950.
- [55] M. B. Ketchen, D. Grischkowsky, T. C. Chen, C. C. Chi, I. N. Duling, N. J. Halas, *et al.*, "Generation of Subpicosecond Electrical Pulses on Coplanar Transmission-Lines," *Applied Physics Letters*, vol. 48, pp. 751-753, Mar 24 1986.
- [56] M. van Exter, C. Fattinger, and D. Grischkowsky, "Terahertz time-domain spectroscopy of water vapor," *Opt Lett*, vol. 14, pp. 1128-1130, 1989.

- [57] M. van Exter and D. R. Grischkowsky, "Characterization of an Optoelectronic Terahertz Beam System," *IEEE Transactions on Microwave Theory and Techniques*, vol. 38, pp. 1684-1691, Nov 1990.
- [58] J. Homola, "Electromagnetic Theory of Surface Plasmons," in *Surface Plasmon Resonance Based Sensors*, ed New York: Springer Berlin Heidelberg, 2006, pp. 3-44.
- [59] A. Kern and M. Walther, "Subgridding in the finite-difference time-domain method for simulating the interaction of terahertz radiation with metal," *Journal of the Optical Society of America B-Optical Physics*, vol. 25, pp. 279-285, Mar 2008.
- [60] A. Taflove and S. C. Hagness, *Computational electrodynamics* vol. 160: Artech house BostonLondon, 2000.
- [61] A. Vial and T. Laroche, "Description of dispersion properties of metals by means of the critical points model and application to the study of resonant structures using the FDTD method," *Journal of Physics D-Applied Physics*, vol. 40, pp. 7152-7158, Nov 21 2007.
- [62] A. Vial, T. Laroche, M. Dridi, and L. Le Cunff, "A new model of dispersion for metals leading to a more accurate modeling of plasmonic structures using the FDTD method," *Applied Physics a-Materials Science & Processing*, vol. 103, pp. 849-853, Jun 2011.
- [63] A. Ivinskaya, "Finite-Difference Frequency-Domain Method in Nanophotonics," Department of Photonics Engineering, Technical University of Denmark (DTU), Kgs. Lyngby, Denmark, 2011.
- [64] U. S. Inan and R. A. Marshall, *Numerical Electromagnetics: The FDTD Method*: Cambridge University Press, 2011.
- [65] A. Z. Elsherbeni and V. Demir, *The finite-difference time-domain method for electromagnetics with MATLAB simulations*: SciTech Pub., 2009.
- [66] J. Bravo-Abad, F. J. Garcia-Vidal, and L. Martin-Moreno, "Resonant transmission of light through finite chains of subwavelength holes in a metallic film," *Physical Review Letters*, vol. 93, p. 227401, Nov 26 2004.

- [67] Q. J. Wang, J. Q. Li, C. P. Huang, C. Zhang, and Y. Y. Zhu, "Enhanced optical transmission through metal films with rotation-symmetrical hole arrays," *Applied Physics Letters*, vol. 87, p. 091105, Aug 29 2005.
- [68] S. H. Yang and P. R. Bandaru, "Effect of surface texture and geometry on spoof surface plasmon dispersion," *Optical Engineering*, vol. 47, p. 029001, Feb 2008.
- [69] D. Z. Han, F. Q. Wu, X. Li, C. Xu, X. H. Liu, and J. Zia, "Transmission and absorption of metallic films coated with corrugated dielectric layers," *Applied Physics Letters*, vol. 89, p. 091104, Aug 28 2006.
- [70] Z. B. Li, J. G. Tian, W. Y. Zhou, W. P. Zang, and C. Zhang, "Periodic dielectric bars assisted enhanced transmission and directional light emission from a single subwavelength slit," *Opt Express*, vol. 14, pp. 8037-42, Sep 4 2006.
- [71] M. J. A. de Dood, E. F. C. Driessen, D. Stolwijk, M. P. van Exter, M. A. Verschuuren, and G. W. t. Hooft, "Index Matching of Surface Plasmons," in *Metamaterials III*, Strasbourg, France, 2008.
- [72] M. J. A. de Dood, E. F. C. Driessen, D. Stolwijk, M. A. Vershuuren, and G. W. t. Hooft, "Coupling Surface Plasmons: Index matching and Dielectric Pillar Arrays," in *Quantum Electronics and Laser Science Conference (QELS)*, San Jose, California, 2008.
- [73] M. de Dood, E. Driessen, D. Stolwijk, and M. van Exter, "Observation of coupling between surface plasmons in index-matched hole arrays," *Physical Review B*, vol. 77, 2008.
- [74] D. Stolwijk, E. F. C. Driessen, M. A. Verschuuren, G. W. t Hooft, M. P. van Exter, and M. J. A. de Dood, "Enhanced coupling of plasmons in hole arrays with periodic dielectric antennas," *Optics Letters*, vol. 33, p. 363, 2008.
- [75] W. Zhou and T. W. Odom, "Tunable subradiant lattice plasmons by out-of-plane dipolar interactions," *Nat Nanotechnol*, vol. 6, pp. 423-7, Jul 2011.

- [76] T. W. Odom, H. W. Gao, J. M. McMahon, J. Henzie, and G. C. Schatz, "Plasmonic superlattices: Hierarchical subwavelength hole arrays," *Chemical Physics Letters*, vol. 483, pp. 187-192, Dec 1 2009.
- [77] G. Kichin, T. Weiss, H. Gao, J. Henzie, T. W. Odom, S. G. Tikhodeev, *et al.*, "Metal–dielectric photonic crystal superlattice: 1D and 2D models and empty lattice approximation," *Physica B: Condensed Matter*, vol. 407, pp. 4037-4042, 2012.
- [78] R. Taubert, "From near-field to far-field: plasmonic coupling in three-dimensional nanostructures," Doctoral Dissertation, University of Stuttgart, 2012.
- [79] H. Wang, D. W. Brandl, P. Nordlander, and N. J. Halas, "Plasmonic nanostructures: artificial molecules," *Acc Chem Res*, vol. 40, pp. 53-62, Jan 2007.
- [80] U. Fano, "Effects of Configuration Interaction on Intensities and Phase Shifts," *Physical Review*, vol. 124, pp. 1866-1878, 1961.
- [81] J. F. O'Hara, E. Smirnova, A. K. Azad, H.-T. Chen, and A. J. Taylor, "Effects of Microstructure Variations on Macroscopic Terahertz Metafilm Properties," *Active and Passive Electronic Components*, vol. 2007, pp. 1-10, 2007.
- [82] F. Hao, Y. Sonnefraud, P. Van Dorpe, S. A. Maier, N. J. Halas, and P. Nordlander, "Symmetry breaking in plasmonic nanocavities: subradiant LSPR sensing and a tunable Fano resonance," *Nano Lett*, vol. 8, pp. 3983-8, Nov 2008.
- [83] J. B. Lassiter, H. Sobhani, J. A. Fan, J. Kundu, F. Capasso, P. Nordlander, *et al.*, "Fano resonances in plasmonic nanoclusters: geometrical and chemical tunability," *Nano Lett*, vol. 10, pp. 3184-9, Aug 11 2010.
- [84] B. Gallinet and O. J. Martin, "Influence of electromagnetic interactions on the line shape of plasmonic Fano resonances," *ACS Nano*, vol. 5, pp. 8999-9008, Nov 22 2011.
- [85] Y. Francescato, V. Giannini, and S. A. Maier, "Plasmonic systems unveiled by Fano resonances," *ACS Nano*, vol. 6, pp. 1830-8, Feb 28 2012.

- [86] F. Wen, J. Ye, N. Liu, P. Van Dorpe, P. Nordlander, and N. J. Halas, "Plasmon transmutation: inducing new modes in nanoclusters by adding dielectric nanoparticles," *Nano Lett*, vol. 12, pp. 5020-6, Sep 12 2012.
- [87] M. Hentschel, D. Dregely, R. Vogelgesang, H. Giessen, and N. Liu, "Plasmonic oligomers: the role of individual particles in collective behavior," *ACS Nano*, vol. 5, pp. 2042-50, Mar 22 2011.
- [88] M. Nieto-Vesperinas, *Scattering and Diffraction in Physical Optics*. Singapore: World Scientific Publishing Co. Pte. Ltd., 2006.
- [89] S.-H. Yang and P. R. Bandaru, "Effect of surface texture and geometry on spoof surface plasmon dispersion," *Optical Engineering*, vol. 47, p. 029001, 2008.
- [90] E. Stone and E. Hendry, "Dispersion of spoof surface plasmons in open-ended metallic hole arrays," *Physical Review B*, vol. 84, 2011.
- [91] B. Gralak, S. Enoch, and G. Tayeb, "Anomalous refractive properties of photonic crystals," *J Opt Soc Am A Opt Image Sci Vis*, vol. 17, pp. 1012-20, Jun 2000.
- [92] J. D. Joannopoulos, S. G. Johnson, J. N. Winn, and R. D. Meade, *Photonic Crystals: Molding the Flow of Light*, 2 ed.: Princeton University Press, 2008.
- [93] L. Feng, M.-H. Lu, V. Lomakin, and Y. Fainman, "Plasmonic photonic crystal with a complete band gap for surface plasmon polariton waves," *Applied Physics Letters*, vol. 93, p. 231105, 2008.
- [94] "Negative Thick Resists," ed: Futurrex, Inc.
- [95] M. T. Reiten, "Spatially Resolved Terahertz Propagation," Doctoral Thesis, Electrical Engineering, Oklahoma State University, Stillwater, OK, 2006.
- [96] B. E. A. Saleh and M. C. Teich, *Fundamentals of Photonics*. Hoboken, New Jersey: John Wiley & Sons, Inc., 2007.
- [97] J. Alda, "Laser and Gaussian beam propagation and transformation," in *Encyclopedia of Optical Engineering*, ed New York: Marcel Dekker Inc, 2003.

- [98] J.-B. Masson, A. Podzorov, and G. Gallot, "Extended Fano model of Extraordinary Electromagnetic Transmission through subwavelength hole arrays in the terahertz domain," *Optics Express*, vol. 17, pp. 15280–15291, 2009.
- [99] A. Miroshnichenko, S. Flach, and Y. Kivshar, "Fano resonances in nanoscale structures," *Reviews of Modern Physics*, vol. 82, pp. 2257-2298, 2010.

VITA

Brady Andrew Whisenhunt

Candidate for the Degree of

Master of Science

Thesis: TERAHERTZ TRANSMISSION ENHANCEMENT IN FINITE-SIZE
ARRAYS OF SUBWAVELENGTH HOLES MODIFIED WITH
DIELECTRIC PEG LAYER

Major Field: Electrical Engineering

Biographical:

Education:

Completed the requirements for the Master of Science in Electrical Engineering at Oklahoma State University, Stillwater, Oklahoma in May, 2013.

Completed the requirements for the Bachelor of Science in Electrical Engineering at Oklahoma State University, Stillwater, Oklahoma in 2005.

Experience:

Employed as Electrical Engineer at Frontier Electronic Systems (FES) in Stillwater, Oklahoma, 2005 to present.

Professional Memberships:

Member of The Optical Society of America (OSA), 2009-present.